Article

Cell

General Anesthesia Decouples Cortical Pyramidal Neurons

Graphical Abstract

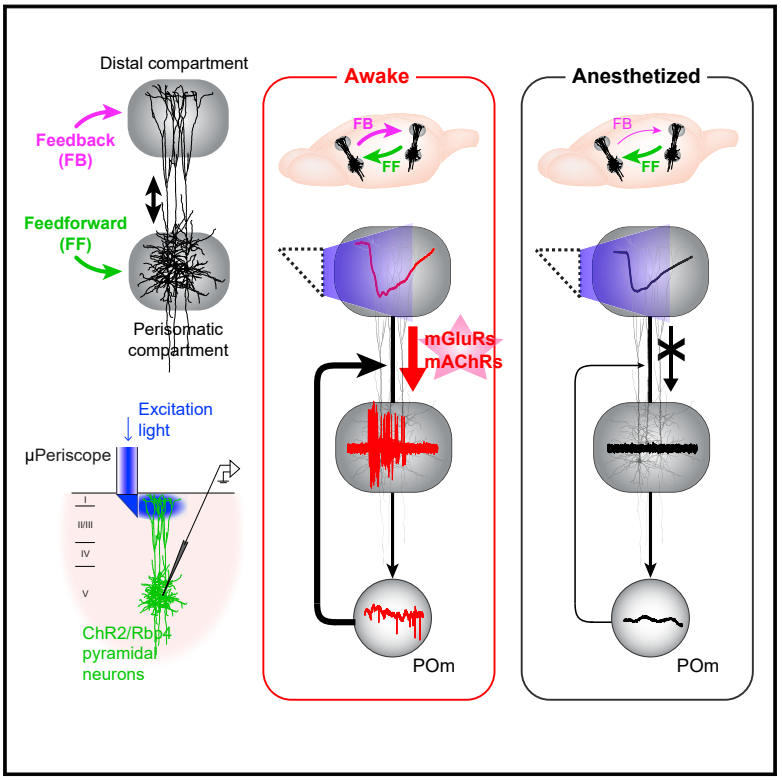

Authors

Mototaka Suzuki, Matthew E. Larkum

Correspondence

mototaka@gmail.com

In Brief

Suzuki and Larkum demonstrate, in the mouse somatosensory cortex, that general anesthesia decouples the flow of information between layer 5 pyramidal neuron dendrites and their cell bodies, providing a cellular mechanism that unifies two theories of consciousness.

Highlights

- Anesthesia decouples signaling along apical dendrites of layer 5 pyramidal neurons
- This suppresses the influence of feedback arriving at the distal dendrites
- mAChRs and thalamic activation of mGluRs are necessary for coupling
- The mechanism reconciles two competing explanations for the action of anesthesia

Suzuki & Larkum, 2020, Cell *180*, 666–676
February 20, 2020
https://doi.org/10.1016/j.cell.2020.01.024

CellPress

Cell

Article

General Anesthesia Decouples Cortical Pyramidal Neurons

Mototaka Suzuki[1,2,*] and Matthew E. Larkum[1]
[1]NeuroCure Cluster of Excellence, Institute for Biology, Humboldt University of Berlin, Chariteplatz 1, 10117 Berlin, Germany
[2]Lead Contact
*Correspondence: mototaka@gmail.com
https://doi.org/10.1016/j.cell.2020.01.024

SUMMARY

The mystery of general anesthesia is that it specifically suppresses consciousness by disrupting feedback signaling in the brain, even when feedforward signaling and basic neuronal function are left relatively unchanged. The mechanism for such selectiveness is unknown. Here we show that three different anesthetics have the same disruptive influence on signaling along apical dendrites in cortical layer 5 pyramidal neurons in mice. We found that optogenetic depolarization of the distal apical dendrites caused robust spiking at the cell body under awake conditions that was blocked by anesthesia. Moreover, we found that blocking metabotropic glutamate and cholinergic receptors had the same effect on apical dendrite decoupling as anesthesia or inactivation of the higher-order thalamus. If feedback signaling occurs predominantly through apical dendrites, the cellular mechanism we found would explain not only how anesthesia selectively blocks this signaling but also why conscious perception depends on both cortico-cortical and thalamo-cortical connectivity.

INTRODUCTION

The fundamental conundrum of anesthesia is that although there can be a total disruption of consciousness, there are very few direct effects on the basic firing properties of neurons (Alkire et al., 2008). It has been observed that anesthesia is associated with a decrease in feedback effectiveness throughout the cortex (Figure 1A, top; Lee et al., 2013; Mashour, 2014). Notably, cortical pyramidal neurons play a central role in feedback signaling between brain areas (Harris and Shepherd, 2015; Figure 1A, bottom left) because their distal apical dendrites in layer 1 (L1) receive a large fraction of cortical feedback connections (Larkum, 2013). It has been hypothesized that the action of anesthesia might be downregulation of the distal dendritic compartment in layer 5 (L5) pyramidal neurons (Llinás and Ribary, 2001; Meyer, 2015). It is also possible that the influence of feedback signals could be affected by regulation of the coupling between these two compartments (Figure 1A, black arrow).

To investigate this question, we optogenetically generated a depolarization in the distal apical dendrites of L5 pyramidal neurons, mimicking feedback input to L1 of the neocortex (Figure 1A, bottom right). Using this "forward" approach (Hallez et al., 2007), we kept the influence of feedback to dendrites constant, allowing us to concentrate on the cellular as opposed to the network effects of anesthesia. The light-activatable cation channel channelrhodopsin 2 (ChR2) (Boyden et al., 2005; Nagel et al., 2003) was expressed in L5 pyramidal neurons, and light was delivered to the distal apical dendrites using a micro-optical tool (μPeriscope; Suzuki and Larkum, 2017) capable of layer-specific light illumination (Figure 1A, bottom right). We combined this with sequential, layer-specific electrical recordings using glass pipettes at variable depths (Figure 1A, bottom right). ChR2 was expressed in L5 pyramidal neurons via injection of the adeno-associated virus (AAV) construct to L5 of the primary somatosensory cortex in an *Rbp4-Cre* transgenic mouse line (Figure 1B) where Cre recombinase is predominantly expressed in L5 pyramidal neurons (Beltramo et al., 2013; Gong et al., 2007). Using the μPeriscope, we could deliver a narrow beam of light (~200–250 μm; Suzuki and Larkum, 2017) to the upper layers, which caused depolarization specifically in the distal dendrites of L5 pyramidal neurons expressing ChR2 (Figure 1C). This approach provided a precise measurement of the dipole created across L5 pyramidal neurons that has long been thought to be the major contributing factor to electroencephalogram (EEG) and other extracellular recording methods (Einevoll et al., 2013). The response evoked by optogenetically depolarizing the dendrites was equivalent to the sensory responses over reasonable stimulus intensities (Figure S1A). By switching gaseous isoflurane anesthesia on and off, we could manipulate the animals' conscious state (Figure S1B; Ferezou et al., 2007; Haider et al., 2013; McGinley et al., 2015) while leaving other experimental conditions (e.g., the μPeriscope and electrodes) unchanged.

RESULTS

Interestingly, we did not observe a marked difference in the dendritic response to optogenetic stimulation of distal apical dendrites in the awake state versus the anesthetized state (Figure 1D top left; see Figure S1C for the grand average). We expect that the overwhelming effect of the current through ChR2 channels masked any non-linearity because of other conductances. Strikingly, however, the somatic response recorded in L5 was markedly different depending on the brain

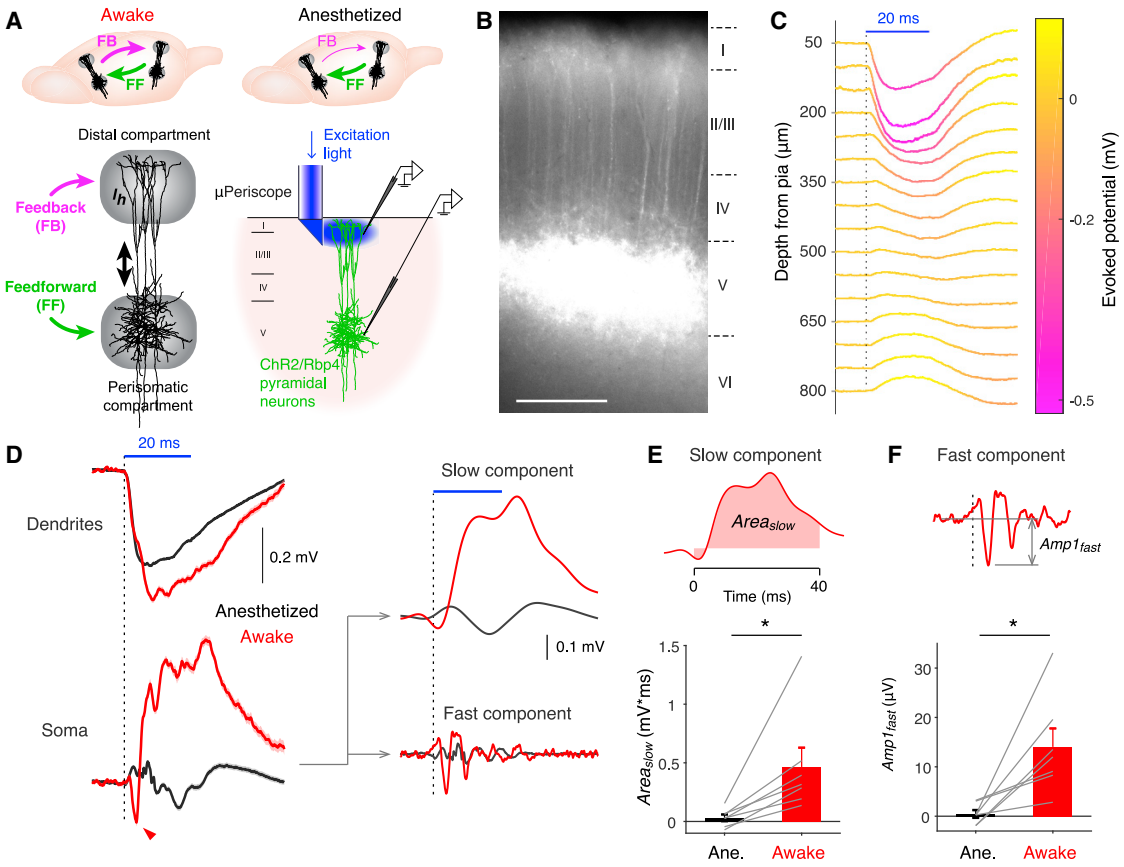

Figure 1. Anesthesia Decouples Dendro-somatic Signaling in Cortical L5 Pyramidal Neurons

(A) The problem and approach of the present study. Paradoxically, anesthesia selectively disrupts feedback signaling (top). L5 pyramidal neurons are hypothesized to play an important role because they receive feedback signals at the distal compartment and feedforward signals at the perisomatic comportment (bottom left). Our approach is to optogenetically stimulate the distal compartment specifically while measuring propagation of the activity to the perisomatic compartment (bottom right).

(B) A fluorescence image of the cortical slice where L5 pyramidal neurons express ChR2 and yellow fluorescent protein (YFP). Scale bar, 200 µm.

(C) Field potentials evoked by optogenetic stimulation of distal apical dendrites during 1% isoflurane anesthesia. The blue bar indicates the timing of blue light. Each trace represents the average over 50–70 measurements.

(D) Optogenetically evoked dendritic and somatic potentials during anesthesia and wakefulness (left). Somatic potentials are decomposed into fast and slow components (right).

(E and F) Both fast (F) and slow (E) components are significantly enhanced during wakefulness (awake) compared with anesthesia (Ane.) (n = 7 mice, both $p < 0.05$, Wilcoxon signed-rank test). Error bars indicate SEM.

state (Figure 1D, bottom left). Decomposing the somatic response to high- and low-frequency components (Figure 1D, right), we found that both components were almost completely abolished in the anesthetized state (Figures 1E and 1F; both $p < 0.05$, Wilcoxon signed-rank test, n = 7 mice), implying that anesthesia significantly decouples the signaling from the distal dendrite to the soma across L5 neurons. The high-frequency component showed spike-like events reminiscent of a population spike with multiple action potentials (APs). The first somatic spike-like event (red arrow in Figure 1D, bottom left) came with short latency (5.9 ± 0.4 ms, mean ± SEM; n = 7 mice) after the onset of light given to the distal apical dendrites, suggesting that the dendritic compartment is very well coupled to the somatic compartment in the awake state. The amplitude of the dendritic response increased proportionally to the light intensity of the stimulus (Figures S1D and S1E) in both awake and anesthetized states. However, although both components of the somatic response also increased proportionally to the stimulus intensity under awake conditions, the somatic response was largely independent of the stimulus intensity under anesthetized conditions (Figures S1D and S1E), consistent with powerful decoupling of the soma from the distal dendritic compartment. This effect was equivalent with different anesthetic agents with very different molecular targets (isoflurane, ketamine/xylazine, and urethane; Figure S1F), suggesting that the coupling of distal and proximal compartments across pyramidal neurons might be a general target of anesthesia. This state-dependent change of coupling was also observed in other cortical areas (Figures S2A–S2D), suggesting the generality of this finding over the neocortex. On the other hand, L2/3 pyramidal neurons did not exhibit this state-dependent change of coupling (Figures S2E and S2F).

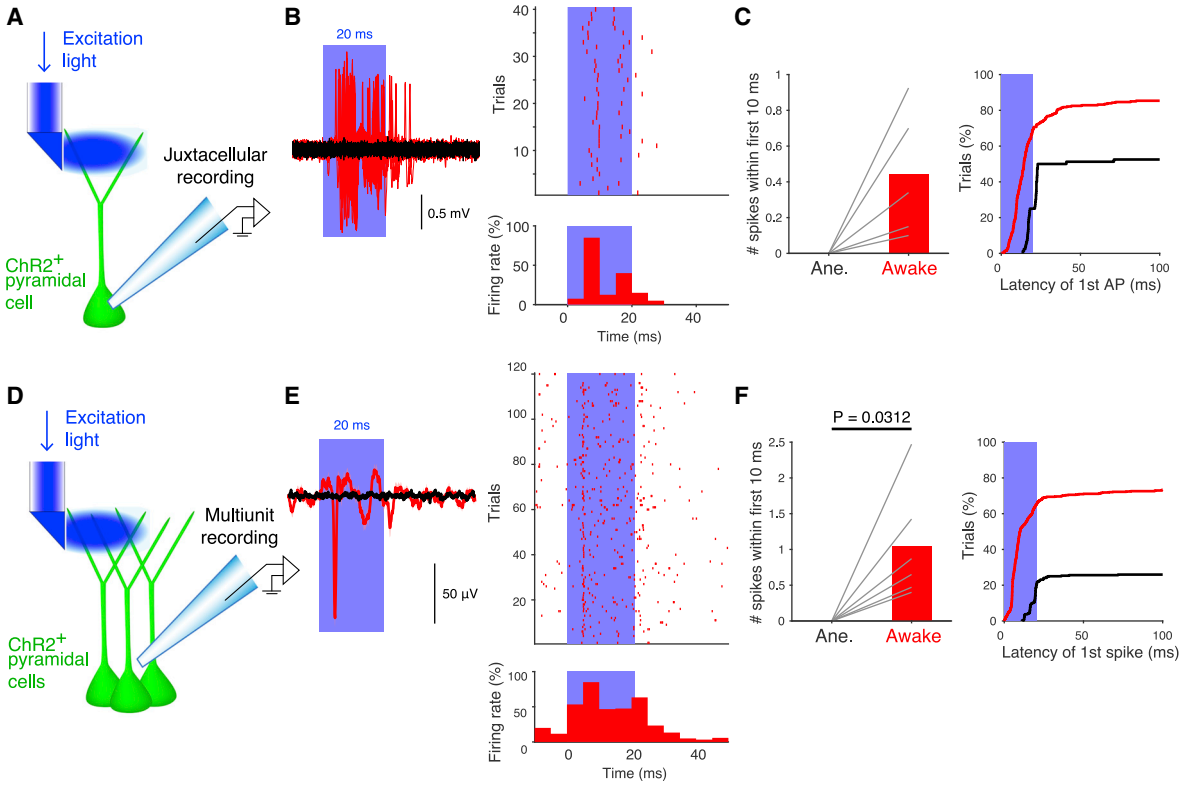

Figure 2. Somatic APs Underlie the Fast Somatic Component during Wakefulness

(A) Schematic diagram of the juxtacellular recording from a ChR2$^+$ L5 pyramidal neuron.

(B) Left: an example neuron evoking somatic APs only during wakefulness upon optogenetic stimulation of distal apical dendrites. Right: the corresponding raster plot of APs (top) and histogram (bottom).

(C) Left: in all 5 neurons, the number of APs evoked within 10 ms after light onset increased during wakefulness. Right: cumulative plot of the latency of the first AP during anesthesia and wakefulness (pooled data from 5 neurons).

(D) Schematic diagram of the multiunit recording from ChR2$^+$ L5 pyramidal neurons.

(E) Left: evoked multiunit responses during wakefulness upon optogenetic stimulation of distal apical dendrites. Right: the corresponding raster plot of spikes (top) and histogram (bottom).

(F) Left: in all 6 mice, the number of spikes evoked within 10 ms after light onset increased during wakefulness ($p = 0.0312$, Wilcoxon signed-rank test, $n = 6$ mice). Right: cumulative plot of the latency of the first spike during both anesthesia and wakefulness (pooled data from 6 mice).

Next we tested whether enhanced coupling reflected output APs at the somata of pyramidal neurons. Using the "opto-patcher" method (Katz et al., 2013; Muñoz et al., 2014) involving single-cell juxtacellular recordings, we recorded APs directly from identified ChR2-positive L5 pyramidal cells (Figures 2A and S3). These recordings showed fast-evoked and stereotypically timed somatic APs during wakefulness versus reduced and delayed somatic APs during anesthesia (Figures 2B and 2C). Consistent with the identified single-cell recordings, multi-unit activity was also significantly higher in L5 because of optogenetic activation of dendrites during wakefulness compared with anesthetized states ($p = 0.0312$, Wilcoxon signed-rank test, $n = 6$ mice; Figures 2D–2F). Consistent with these data, we found that microinjection of the sodium channel blocker tetrodotoxin (TTX, 3 µM, 50 nL) into L5 also abolished the fast somatic component (all $p < 0.05$ in 3 mice, two-sided Wilcoxon rank-sum test; Figures S4A–S4C). We conclude that the events underlying the fast component were somatic APs of L5 pyramidal neurons.

We were concerned that light activation of the distal dendrites might activate antidromic APs in the axons of L5 cells in the upper layers. To test this, we created definitive axonal input using *trans*-callosal activation of axons from the same neurons with light in the contralateral hemisphere. This showed delayed response in L5 (Figures S4D–S4G) that was much weaker than the response to direct dendritic depolarization (Figures 1D–1F). Importantly, antidromic APs caused very similar somatic responses in both the awake and anesthetized states. Moreover, we repeated the original experiment, depolarizing dendrites with light using another transgenic mouse line, *Sim1-Cre*, which expresses Cre recombinase in a subset of L5 neurons, pyramidal tract (PT) neurons in L5b, which predominantly project subcortically with significantly fewer axons in L1 and L2 compared with other L5 cells (Brown and Hestrin, 2009; Harris and Shepherd, 2015; Kim et al., 2015). Even in Sim1-Cre mice, we consistently observed wakefulness-enhanced somatic responses upon dendritic stimulation ($p = 0.0312$, two-sided Wilcoxon signed-rank test, $n = 6$ mice; Figures S4H and S4I). Collectively, these data

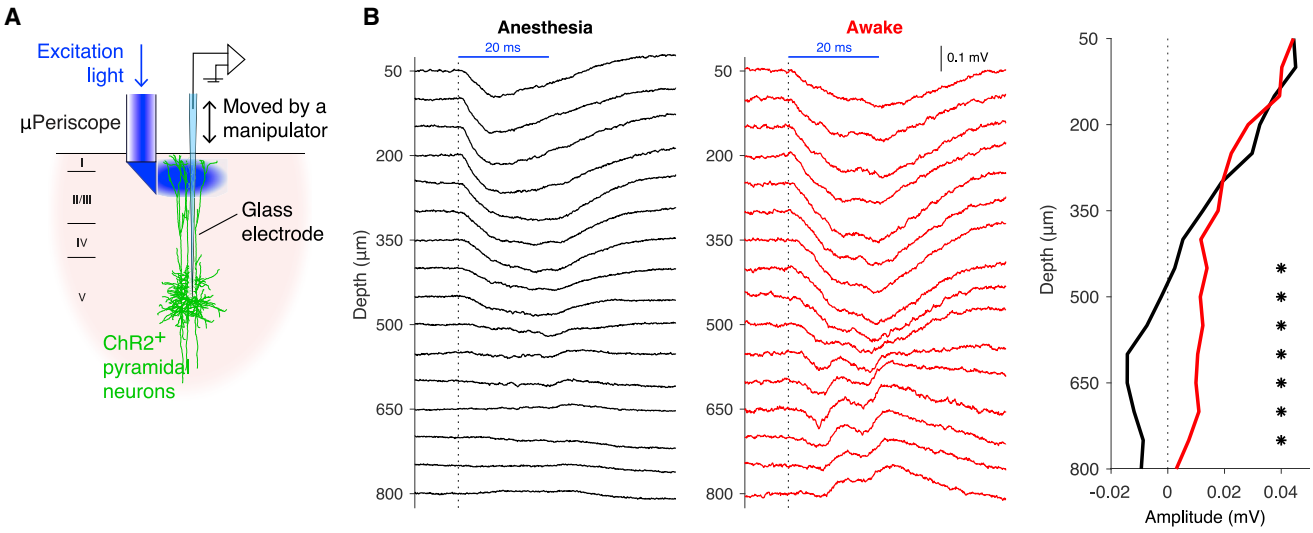

Figure 3. Propagation of Dendro-somatic Signals Fails in the Proximal Apical Region during Anesthesia

(A) Schematic diagram of the experiment.

(B) Optogenetically evoked field potentials during anesthesia (left) and wakefulness (center). Average potentials at the peak somatic response are overlaid (n = 5 mice, right). *p < 0.05, Wilcoxon signed-rank test. Shading indicates SD.

indicate that antidromic activation of APs evokes only a small delayed population signal in L5 in both anesthetized and awake states. Antidromic Aps, therefore, did not contribute significantly to the overall signal and were not characterized by fast, stereotypically timed APs. On the other hand, dendritic depolarization is known to evoke somatic APs with stereotypical timing in short high-frequency bursts (Williams and Stuart, 1999). We conclude that anesthesia prevents dendritic depolarization from generating somatic APs and, therefore, the effectiveness of feedback input arriving at the distal dendrites. We define "coupling" as the effect of dendritic depolarization on the generation of somatic APs; therefore, from here on, we focus mainly on the fast component. Note, however, that the changes in the fast component always correlated with changes in the slow component.

What underlies decoupling of the signals along the apical dendritic axis (Figure 1A)? To investigate this, we measured the profile of dendritic responses and the propagation of signals along apical dendrites during wakefulness and anesthesia using a finer resolution of recording positions (50-μm intervals; Figures 3A and 3B). This profile confirmed that dendritic responses reliably propagated to the soma and evoked fast spikes during wakefulness (Figure 3B, awake) but were significantly attenuated with late (>10 ms after light onset), if any, somatic APs during anesthesia (Figure 3B, anesthesia). Averaging across recordings for each depth revealed that the signal was not dependent on brain state for recordings close to dendrites but began to diverge in the proximal region of apical shaft dendrites around a depth of 400–450 μm (Figure 3B, right), confirming that the mechanism for decoupling signals under anesthesia did not act directly on the distal dendritic compartment but, rather, on the propagation of signals to cell bodies. Consistent with this interpretation, we found that antagonists of L-type Ca^{2+} and NMDA channels did not significantly reduce generation of APs at the cell body (Figures 4A–4C). Here, an L-type Ca^{2+} channel blocker (nifedipine, 43 μM, 50 nL) and an NMDA receptor blocker (APV, 500 μM, 50 nL) injected to superficial layers significantly reduced the dendritic responses ($p < 0.05$ in all 3 mice for APV and in 3 of 4 mice for nifedipine, Wilcoxon rank-sum test; Figure 4C); however, they did not impair the fast somatic component (all $p > 0.05$, Wilcoxon rank-sum test, n = 3 mice for both APV and nifedipine; Figure 4B).

It has been shown *in vitro* that coupling of the dendritic and somatic compartments in L5 pyramidal neurons is extremely sensitive to the depolarization state of the proximal apical dendrite (Larkum et al., 2001; Schaefer et al., 2003). It is therefore possible that depolarization caused during the awake state is responsible for the enhanced coupling between the dendritic and somatic compartments. On the other hand, anesthesia is often characterized by slow alternation between so-called up and down states (Wilson and Kawaguchi, 1996). Up states are commonly assumed to resemble awake states because cells are significantly depolarized in both states (Alkire et al., 2008; Constantinople and Bruno, 2011; Destexhe et al., 2003). However, we found that decoupling of the dendritic and somatic compartments associated with anesthesia continued to be effective in both up and down states (Figures S5A–S5C), and both were significantly different from the robust coupling in the awake state (both $p < 0.05$, Kruskal-Wallis test with post hoc multiple comparisons, n = 5 mice; Figure S5D). This is consistent with the fact that up states do not lead to consciousness and suggests that coupling of feedback signals through L5 pyramidal neurons is not simply a function of the depolarization state of the neurons. We also tested whether the type of awake state was a determining factor by comparing the change in coupling between two awake states—actively behaving versus quietly

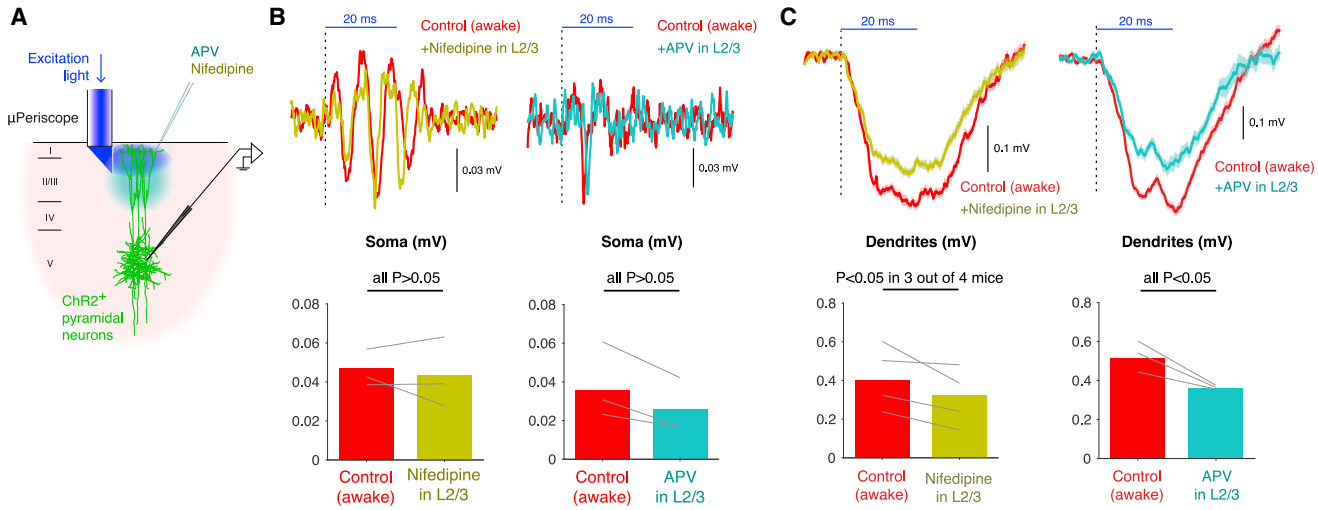

Figure 4. Coupling Does Not Depend on Distal Dendritic NMDA Receptors or L-type Ca^{2+} Channels

(A) Schematic diagram of the pharmacology experiments.

(B) Neither 43 μM nifedipine nor 500 μM APV significantly reduced the fast somatic component (all $p > 0.05$, Wilcoxon rank-sum test, $n = 3$ mice with nifedipine and APV).

(C) Dendritic responses to optogenetic stimulation were significantly reduced by nifedipine (left, $n = 3$ of 4 mice, $p < 0.05$, Wilcoxon rank-sum test) and APV (right, all $n = 3$ mice, $p < 0.05$, Wilcoxon rank-sum test).

resting states—but found no significant difference (all $p > 0.5$, Wilcoxon rank-sum test, $n = 3$ mice; Figures S5E and S5F).

Because depolarization alone was not responsible for the effects we observed on coupling (i.e., the up and down states were equivalent), we looked at the effect of various neuromodulators that have been shown to correlate with the brain state and affect neuronal properties (Constantinople and Bruno, 2011; Labarrera et al., 2018; McCormick, 1993; McGinley et al., 2015; Muñoz et al., 2017; Polack et al., 2013). The neuromodulators acetylcholine (ACh) and noradrenaline (NA) activate not only pyramidal cells (McCormick, 1993; McCormick et al., 1991), in particular distal dendrites (Labarrera et al., 2018; Williams and Fletcher, 2019), but also surrounding dendrite-targeting inhibitory interneurons (Bergles et al., 1996; Muñoz et al., 2017). The net effect of these neuromodulators on dendro-somatic coupling is therefore hard to predict. We measured the somatic response to dendritic stimulation upon pharmacological application of ACh antagonists (both ionotropic and metabotropic) and NA antagonists during the awake state (Figures 5A–5E). Both ACh and NA blockers significantly reduced the amplitude of dendritic responses (Figures 5C and 5E), but, surprisingly, only ACh blockers significantly reduced the wakefulness-enhanced somatic responses (all $p < 0.005$, two-sided Wilcoxon rank-sum test, $n = 4$ mice; Figures 5B and 5D) whereas NA blockers did not (all $p > 0.05$, two-sided Wilcoxon rank-sum test, $n = 4$ mice; Figures 5B and 5D). Again, we interpret the lack of action of the NA blocker to indicate that the artificially induced ChR2 conductance overrides the (known) effect of NA on activity of the distal compartment (Labarrera et al., 2018). We further found that a muscarinic ACh receptor antagonist (1 mM atropine, 50 nL) significantly impaired fast somatic responses whereas a nicotinic ACh receptor antagonist (1 mM mecamylamine, 50 nL) did not (Figures 5F–5J), indicating a significant contribution of muscarinic ACh receptors to enhanced dendro-somatic coupling.

A long-standing hypothesis regarding the action of anesthesia is decoupling of thalamocortical interactions (Alkire et al., 2000; Llinás and Ribary, 2001). This hypothesis appears to be orthogonal to the "cortico-cortical" explanation involving disruption of cortical-cortical feedback (Mashour, 2014). Moreover, the failure of signaling in the bottom third of the apical dendritic axis appears at first glance to be an intrinsically cortical phenomenon. However, this region of the cortex receives a strong projection from higher-order thalamic nuclei that are known to have a neuromodulatory influence because of activation of group I metabotropic glutamate receptors (mGluRs; Sherman, 2014). For the primary somatosensory cortex, the posteromedial nucleus (POm) is an associated higher-order thalamic nucleus that has a significant projection to cortical L5a as well as to L1 (Wimmer et al., 2010; Figure 6A) and is known to play a role in cortical state (Alkire et al., 2000; Llinás and Ribary, 2001). We therefore measured the effect of the mGluR blocker (R,S)-α-methyl-4-carboxyphenylglycine (MCPG; 1.2 mM, 50 nL) and found that local injection of MCPG strikingly impaired coupling, abolishing the somatic response (Figure 6B) while not significantly affecting nearby background activity in the injected region (L2–L4 at 200–500 μm from the pia; $p = 0.625$, Wilcoxon signed-rank test, $n = 5$ mice; Figure 6D). Consistent with this observation, POm activity was significantly elevated during wakefulness compared with anesthetized states (Masri et al., 2008) (all $p < 0.0005$, Wilcoxon signed-rank test, $n = 4$ mice; Figures S6A and S6B), and inactivation of the POm with the $GABA_A$ receptor agonist muscimol (0.5 mM, 50 nL) significantly impaired coupling ($p < 0.05$ in all 4 mice, Wilcoxon rank-sum test; Figures 6E–6H).

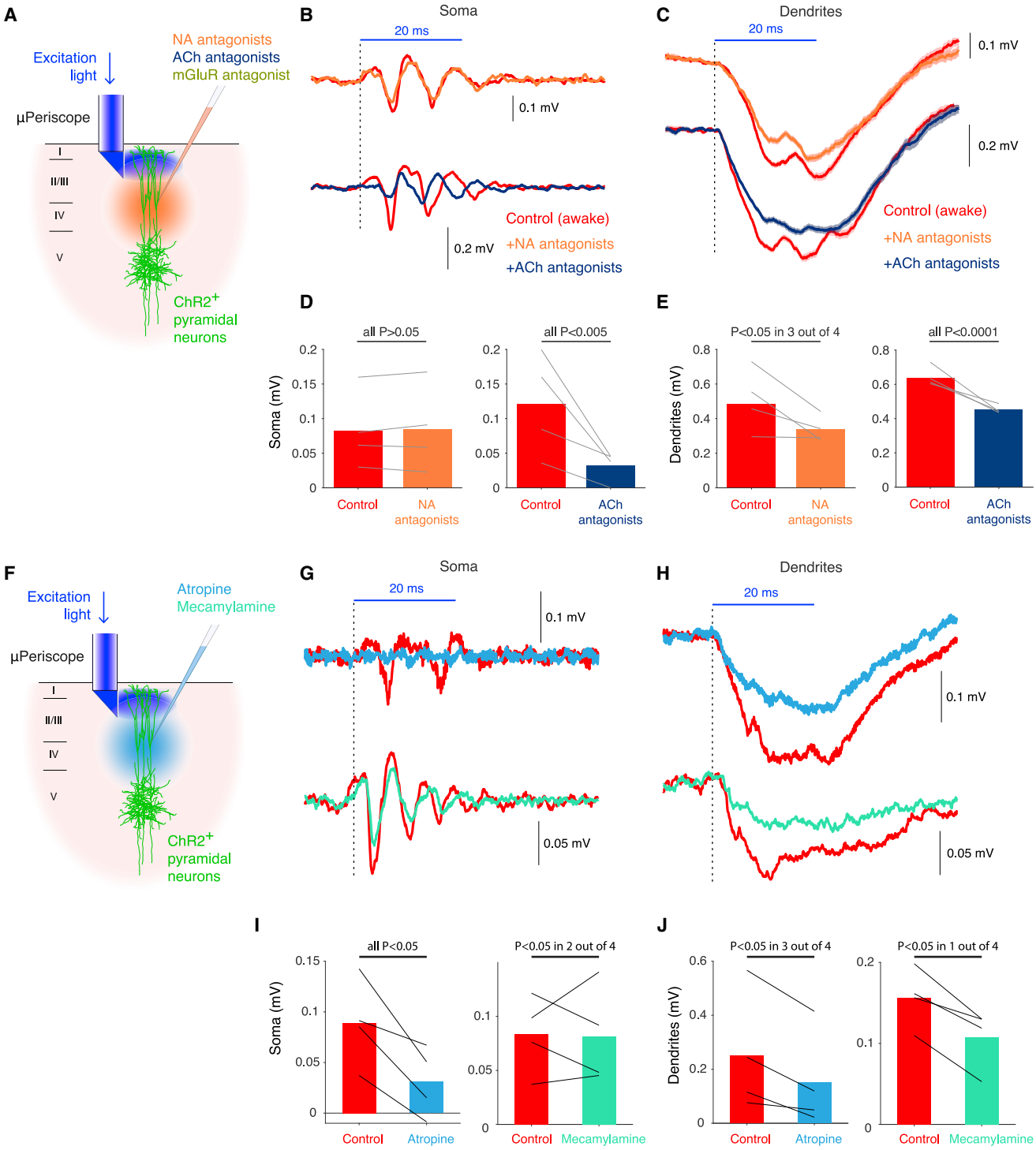

Figure 5. Blocking mAChRs Decouples Cortical L5 Pyramidal Neurons during Wakefulness

(A) Schematic diagram of the pharmacological experiment.

(B) Fast somatic responses before and after ACh antagonists (averaged over 50–70 measurements from one mouse, mean ± SEM) or NA antagonists.

(C) Dendritic responses in the same mouse as shown in (B).

(D) Summary of (B). In all four mice, NA antagonists did not significantly reduce the fast somatic component (all $p > 0.05$, Wilcoxon rank-sum test), whereas ACh antagonists significantly reduced it in all four mice (all $p < 0.005$, Wilcoxon rank-sum test).

(E) Summary of (C). In 3 of 4 mice, NA antagonists significantly reduced the dendritic response ($p < 0.05$, Wilcoxon rank-sum test); in all 4 mice, ACh antagonists significantly reduced dendritic responses (all $p < 0.0001$, Wilcoxon rank-sum test).

(legend continued on next page)

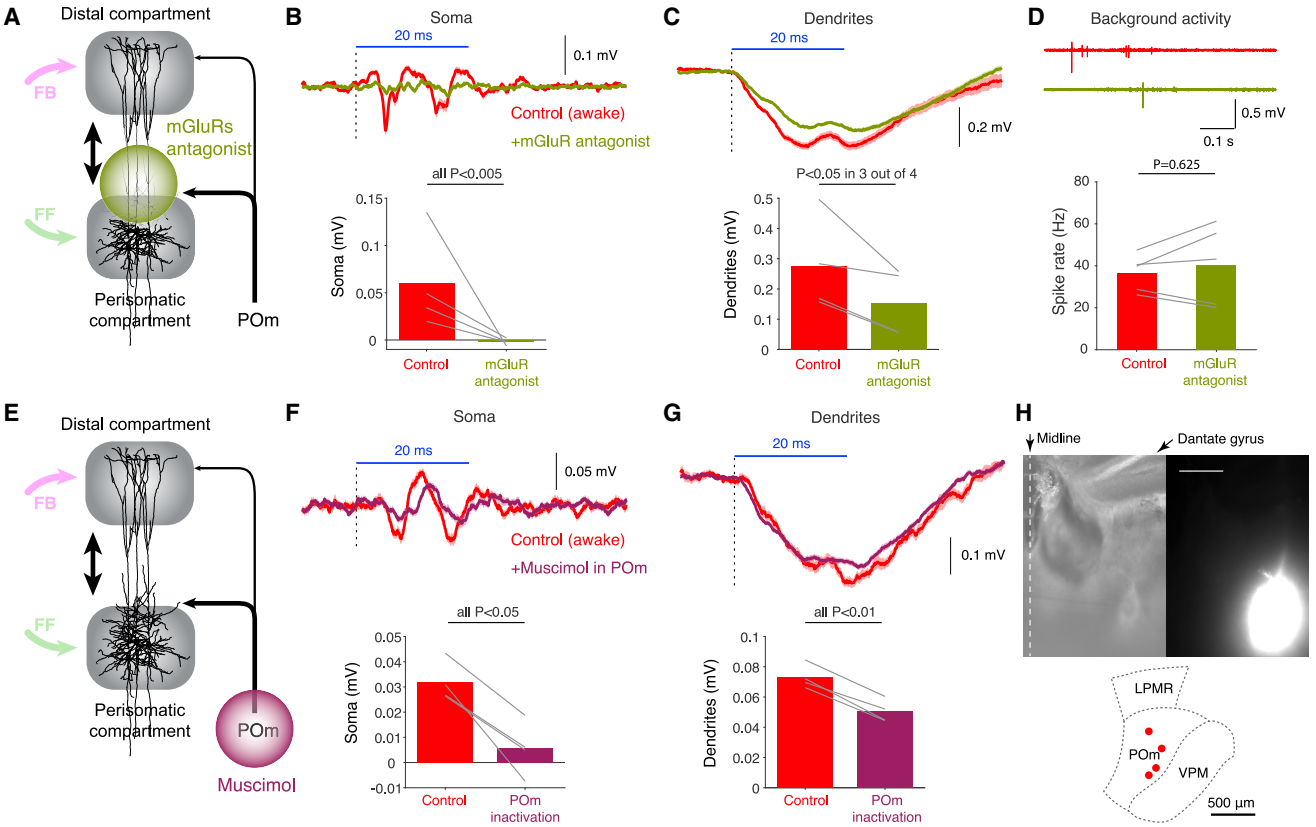

Figure 6. Blocking mGluRs Decouples Cortical L5 Pyramidal Neurons during Wakefulness

(A) Our hypothesis that mGluRs activated by synaptic inputs from the POm may contribute to dendro-somatic coupling of L5 pyramidal neurons.

(B) Top: fast somatic responses before and after the mGluR antagonist MCPG from one mouse. Bottom: in all 4 mice, MCPG significantly reduced the fast somatic response (all $p < 0.005$, Wilcoxon rank-sum test).

(C) Top: dendritic responses before and after the mGluR antagonist MCPG from one mouse. Bottom: in 3 of 4 mice, MCPG significantly reduced dendritic responses (left, $p < 0.05$, Wilcoxon rank-sum test).

(D) Background activity in L2–L4 (200–500 µm below the pia) does not significantly change upon application of an mGluR antagonist (1.2 mM MCPG, 50 nL). Top: representative traces before (red) and after application of MCPG. Bottom: mean spike rate (hertz) of cortical L2–L4 neurons before and after application of MCPG ($p = 0.625$, Wilcoxon signed-rank test, $n = 5$ mice).

(E) Schematic diagram of the experiment.

(F) Top: fast somatic responses before and after muscimol injection to the POm. Bottom: in all four mice, muscimol injection to the POm significantly reduced the fast somatic responses (all $p < 0.05$, Wilcoxon rank-sum test).

(G) Top: dendritic responses before and after muscimol injection to the POm. Bottom: in all 4 mice, muscimol injection to the POm significantly reduced dendritic responses (all $p < 0.01$, Wilcoxon rank-sum test).

(H) Top: bright-field image of the POm and fluorescence image of the same slice. Scale bar, 500 µm. Bottom: measured central locations of fluorescence ($n = 4$ mice). LPMR, lateral posterior medial rostral nucleus; VPM, ventral posteromedial nucleus.

Higher-order thalamic nuclei are known to significantly contribute to conscious perception, attentional control (Saalmann et al., 2012; Schmitt et al., 2017; Zhou et al., 2016), and synaptic plasticity (Gambino et al., 2014; Williams and Holtmaat, 2019). To examine whether anesthetic-induced downregulation is a general characteristic of higher-order thalamic nuclei, we studied another higher-order, visually associated thalamic nucleus, the pulvinar, and, for comparison, the first-order somatosensory thalamic nucleus, the ventral POm (VPM). The pulvinar was downregulated by isoflurane anesthesia (Figures

(F) Schematic diagram of the pharmacological experiment.

(G) Fast somatic responses before and after mACh antagonist (1 mM atropine) (averaged over 50–70 measurements from one mouse, mean ± SEM) or nACh antagonist (1 mM mecamylamine).

(H) Dendritic responses in the same mouse as shown in (G).

(I) Summary of (G). Mecamylamine significantly reduced the fast somatic component in 2 of 4 mice ($p < 0.05$, Wilcoxon rank-sum test), whereas atropine significantly reduced it in all four mice (all $p < 0.05$, Wilcoxon rank-sum test).

(J) Summary of (H). In only 1 of 4 mice, mecamylamine significantly reduced the dendritic response ($p < 0.05$, Wilcoxon rank-sum test). In 3 of 4 mice, atropine significantly reduced dendritic responses ($p < 0.05$, Wilcoxon rank-sum test).

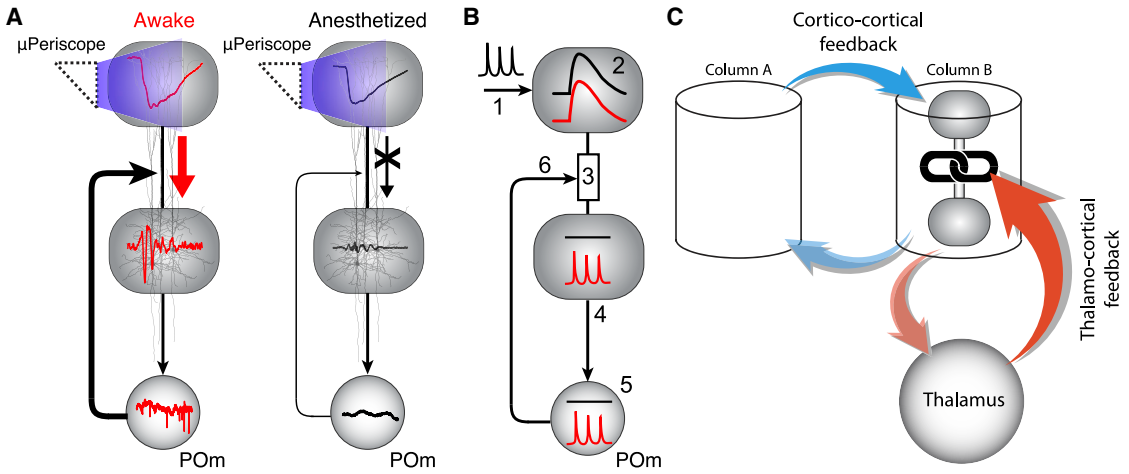

Figure 7. A Theory of General Anesthesia

(A) Graphical summary of the present findings. Optogenetic stimulation of distal apical dendrites resulted in depolarization of dendrites in both anesthetized and awake states. Somatic responses, however, clearly depended on the conscious state. Elevated neuronal activity in the POm during wakefulness correlated with enhanced coupling of L5 pyramidal neurons, and inactivation of the POm during wakefulness significantly impaired coupling.

(B) Our interpretation of the present findings. Feedback signals coming to distal apical dendrites (1) cause equally strong excitatory post-synaptic potentials (2). Because the marked difference in dendro-somatic coupling (3), somatic APs are reliably evoked during wakefulness, whereas delayed and few, if any, APs are evoked during anesthesia (4). Higher POm activity (5) enhances coupling of L5 pyramidal neurons during wakefulness (6).

(C) The model that reconciles the two long-standing hypotheses regarding anesthetic-induced unconsciousness. One hypothesis posits that the cortico-cortical feedback loop is crucial for conscious perception; the other emphasizes the importance of the thalamo-cortical loop. The present findings reveal that decoupling of dendro-somatic compartments of L5 pyramidal neurons results in breakdown of both cortico-cortical and thalamo-cortical feedback loops, providing the cellular mechanism that reconciles the two apparently distinct hypotheses.

S6C and S6D), similarly to the POm, whereas the VPM remained active and strongly responded to a sensory stimulus (air puff) during anesthesia (Figures S6E and S6F), consistent with previous studies (Brecht and Sakmann, 2002; Castro-Alamancos, 2002; Deschênes et al., 2003; Minnery et al., 2003).

The mechanism for anesthesia has often been linked with inhibition because almost all anesthetics upregulate $GABA_A$ receptors (Franks, 2008). In particular, dendrite-targeting somatostatin-positive neurons have been associated with mGluRs (Dalezios et al., 2002; Ferraguti and Shigemoto, 2006). We therefore wondered whether anesthetic-induced decoupling was induced by dendrite-targeting inhibition from somatostatin-positive (SOM^+) interneurons. We tested this possibility by expressing inhibitory DREADD (hM4D(Gi)) (Krashes et al., 2011) in SOM^+ interneurons (Figures S7A and S7B) and found that inactivating SOM^+ interneurons did not enhance coupling of pyramidal neurons (Figure S7C). To further examine the contribution of other interneurons, we applied the $GABA_A$ receptor antagonist gabazine (5 µM, 100 nL) or the AMPA receptor antagonist CNQX (100 µM, 100 nL). Neither of these antagonists enhanced coupling of pyramidal neurons (Figures S7D and S7E). Together, these results suggest that the mechanism for decoupling during anesthesia does not depend on interneurons. However, we do not exclude the possibility that interneurons nevertheless have an influence on dendritic excitability per se because there may be other circuit mechanisms that can explain the observations above. For instance, they might exert dendritic branch-specific (Cichon and Gan, 2015) or dendritic region-specific modulation (Muñoz et al., 2017; Murayama et al., 2009).

DISCUSSION

The present results show that wakefulness makes activation of distal dendrites highly effective in generating somatic APs (Figure 7A), indicating enhanced dendrite-to-soma coupling. We controlled activation of distal dendrites using an optogenetic approach (Figure 7A, µPeriscope) bypassing the difficulty of controlling feedback connectivity. Interestingly, the current sink created by light-activated depolarization of the distal dendritic compartment was very similar under anesthetized and awake conditions (Figure 7A, top). It is possible that anesthesia normally suppresses the dendritic compartment directly (Potez and Larkum, 2008) but that, using the approach taken here, the currents generated by activation of ChR2 masked these effects. If so, then it would mean that the effect of anesthesia on signaling of the tuft to the soma would normally be even greater; however, anesthesia apparently completely suppresses the effect of optogenetic stimulation in any case. Consistent with this, we saw no difference between the amplitude of the dendritic response during anesthetized and awake states over a range of different light intensities (Figures S1C–S1E). Despite the similarity of dendritic activation, we saw clear differences in the responses of the somatic compartment in the lower cortical layers (Figure 7A, center) as well as a clear difference in spontaneous spiking of neurons in the POm (Figure 7A, bottom). Coupling was most successfully blocked by application of an mGluR blocker (MCPG) but also substantially by blockers of muscarinic (i.e., metabotropic) cholinergic receptors. A previous *in vitro* study has shown that activation of mGluRs mobilizes inositol triphosphate (IP_3) and evokes large Ca^{2+} waves (Larkum et al.,

2003) whose functional role is largely unknown (Ross, 2012). In general, the effects of activating mGluRs is likely to have diverse downstream effects on excitability (Kim et al., 2008; Yu et al., 2018).

The data together suggest that anesthesia disrupts active maintenance of coupling along the apical dendritic axis by metabotropic activity in the proximal dendritic compartment of L5 neurons. In this scenario, if the anesthetic downregulates higher-order thalamic input to the cortex (Figure 7B, 5 and 6), then this would decrease the influence of input (Figure 7B, 1) to the distal compartment of deep-layer pyramidal neurons (Figure 7B, 2) by downregulating coupling between the distal and proximal compartments (Figure 7B, 3). De-coupling of signaling across pyramidal neurons would therefore lead to a decrease in the output of cortical columns because of distal dendritic input (Figure 7B, 4). Because distal dendritic input is dominated by long-range feedback input (Cauller, 1995; Rockland, 1998), the overall effect would be widespread decoupling of feedback throughout the cortex. This scenario is also consistent with the fact that anesthetics do not significantly alter the influence of feedforward sensory input to the cortex (Imas et al., 2005; Lee et al., 2013; Liu et al., 2012) because this pathway should predominantly influence synaptic input to the somatic compartment.

There is so far no consensus about how anesthetics interfere with consciousness (Hudetz, 2012); however, the main two hypotheses posit that either the influence of feedback connectivity in cortico-cortical loops is disrupted (Boly et al., 2011; Mashour, 2014) or that higher-order thalamo-cortical loops are disrupted (Alkire et al., 2008; Llinás and Ribary, 2001; Figure 7C). Here we offer a theory of general anesthesia that reconciles these two competing explanations. The fact that inactivation of POm impaired coupling of cortical L5 pyramidal cells suggests that the contribution of higher-order thalamic nuclei to conscious perception is vital by remotely controlling the sensitivity of cortical pyramidal neurons to feedback signals that arrive at distal apical dendrites. However, in general, the theory rests on the fact that coupling of integration zones along the apical axis of pyramidal neurons is a fulcrum on which a large fraction of long-range cortical connectivity depends. In principle, therefore, according to this theory, any effect brought on by anesthesia that leads to disruption of signaling along this axis would lead to loss of consciousness. This might also explain how different anesthetics with multiple targets all specifically lead to loss of consciousness. It could therefore crucially control factors such as integrated information (or phi; Tononi et al., 2016) while having very little effect on the firing properties of neurons per se, consistent with this major unexplained fact about anesthesia. If so, this would also be relevant to our understanding of consciousness, although we emphasize that this is likely to be far more complex, involving factors not explored in this study. Nevertheless, because the coupling mechanism intrinsically involves the apical dendrites of cortical pyramidal neurons, this explanation of general anesthesia only makes sense in light of a crucial contribution of these dendrites to the operation of the cortex (Larkum, 2013).

STAR★METHODS

Detailed methods are provided in the online version of this paper and include the following:

- KEY RESOURCES TABLE
- LEAD CONTACT AND MATERIALS AVAILABILITY
- EXPERIMENTAL MODEL AND SUBJECT DETAILS
- METHOD DETAILS
  - Virus injection
  - Layer-specific optical stimulation
  - Extracellular recordings
  - Optopatcher recordings
  - Pharmacology
  - Sensory stimulation
- QUANTIFICATION AND STATISTICAL ANALYSIS
- DATA AND CODE AVAILABILITY

ACKNOWLEDGMENTS

The authors thank Jaan Aru, William A. Phillips, Johan Storm, and Naoya Takahashi for comments on an earlier version of the manuscript and Karl Deisseroth and The University of Pennsylvania Vector Core for pAAV.EF1a.DIO.hChR2(H134R)-eYFP.WPRE.hGH (Addgene 20298). The research was supported by the German Research Foundation (EXC 257 NeuroCure, LA 3442/5-1, and 327654276-SFB 1315).

AUTHOR CONTRIBUTIONS

Conceptualization, M.S.; Methodology, M.S. and M.E.L.; Investigation, M.S.; Visualization, M.S. and M.E.L.; Writing – Original Draft, M.S.; Writing – Review & Editing, M.S. and M.E.L.; Funding Acquisition, M.E.L.; Resources, M.E.L.; Supervision, M.E.L.

DECLARATION OF INTERESTS

The authors declare no competing interests.

Received: February 20, 2019
Revised: November 15, 2019
Accepted: January 15, 2020
Published: February 20, 2020

REFERENCES

Alkire, M.T., Haier, R.J., and Fallon, J.H. (2000). Toward a unified theory of narcosis: brain imaging evidence for a thalamocortical switch as the neurophysiologic basis of anesthetic-induced unconsciousness. Conscious. Cogn. *9*, 370–386.

Alkire, M.T., Hudetz, A.G., and Tononi, G. (2008). Consciousness and anesthesia. Science *322*, 876–880.

Beltramo, R., D'Urso, G., Dal Maschio, M., Farisello, P., Bovetti, S., Clovis, Y., Lassi, G., Tucci, V., De Pietri Tonelli, D., and Fellin, T. (2013). Layer-specific excitatory circuits differentially control recurrent network dynamics in the neocortex. Nat. Neurosci. *16*, 227–234.

Bergles, D.E., Doze, V.A., Madison, D.V., and Smith, S.J. (1996). Excitatory actions of norepinephrine on multiple classes of hippocampal CA1 interneurons. J. Neurosci. *16*, 572–585.

Boly, M., Garrido, M.I., Gosseries, O., Bruno, M.A., Boveroux, P., Schnakers, C., Massimini, M., Litvak, V., Laureys, S., and Friston, K. (2011). Preserved feedforward but impaired top-down processes in the vegetative state. Science *332*, 858–862.

Boyden, E.S., Zhang, F., Bamberg, E., Nagel, G., and Deisseroth, K. (2005). Millisecond-timescale, genetically targeted optical control of neural activity. Nat. Neurosci. *8*, 1263–1268.

Brecht, M., and Sakmann, B. (2002). Whisker maps of neuronal subclasses of the rat ventral posterior medial thalamus, identified by whole-cell voltage recording and morphological reconstruction. J. Physiol. *538*, 495–515.

Brown, S.P., and Hestrin, S. (2009). Intracortical circuits of pyramidal neurons reflect their long-range axonal targets. Nature *457*, 1133–1136.

Castro-Alamancos, M.A. (2002). Different temporal processing of sensory inputs in the rat thalamus during quiescent and information processing states in vivo. J. Physiol. *539*, 567–578.

Cauller, L. (1995). Layer I of primary sensory neocortex: where top-down converges upon bottom-up. Behav. Brain Res. *71*, 163–170.

Cichon, J., and Gan, W.B. (2015). Branch-specific dendritic Ca(2+) spikes cause persistent synaptic plasticity. Nature *520*, 180–185.

Constantinople, C.M., and Bruno, R.M. (2011). Effects and mechanisms of wakefulness on local cortical networks. Neuron *69*, 1061–1068.

Dalezios, Y., Luján, R., Shigemoto, R., Roberts, J.D., and Somogyi, P. (2002). Enrichment of mGluR7a in the presynaptic active zones of GABAergic and non-GABAergic terminals on interneurons in the rat somatosensory cortex. Cereb. Cortex *12*, 961–974.

Deschênes, M., Timofeeva, E., and Lavallée, P. (2003). The relay of high-frequency sensory signals in the Whisker-to-barreloid pathway. J. Neurosci. *23*, 6778–6787.

Destexhe, A., Rudolph, M., and Paré, D. (2003). The high-conductance state of neocortical neurons in vivo. Nat. Rev. Neurosci. *4*, 739–751.

Einevoll, G.T., Kayser, C., Logothetis, N.K., and Panzeri, S. (2013). Modelling and analysis of local field potentials for studying the function of cortical circuits. Nat. Rev. Neurosci. *14*, 770–785.

Ferezou, I., Haiss, F., Gentet, L.J., Aronoff, R., Weber, B., and Petersen, C.C. (2007). Spatiotemporal dynamics of cortical sensorimotor integration in behaving mice. Neuron *56*, 907–923.

Ferraguti, F., and Shigemoto, R. (2006). Metabotropic glutamate receptors. Cell Tissue Res. *326*, 483–504.

Franks, N.P. (2008). General anaesthesia: from molecular targets to neuronal pathways of sleep and arousal. Nat. Rev. Neurosci. *9*, 370–386.

Gambino, F., Pagès, S., Kehayas, V., Baptista, D., Tatti, R., Carleton, A., and Holtmaat, A. (2014). Sensory-evoked LTP driven by dendritic plateau potentials in vivo. Nature *515*, 116–119.

Gerfen, C.R., Paletzki, R., and Heintz, N. (2013). GENSAT BAC cre-recombinase driver lines to study the functional organization of cerebral cortical and basal ganglia circuits. Neuron *80*, 1368–1383.

Gong, S., Doughty, M., Harbaugh, C.R., Cummins, A., Hatten, M.E., Heintz, N., and Gerfen, C.R. (2007). Targeting Cre recombinase to specific neuron populations with bacterial artificial chromosome constructs. J. Neurosci. *27*, 9817–9823.

Guo, Z.V., Inagaki, H.K., Daie, K., Druckmann, S., Gerfen, C.R., and Svoboda, K. (2017). Maintenance of persistent activity in a frontal thalamocortical loop. Nature *545*, 181–186.

Haider, B., Häusser, M., and Carandini, M. (2013). Inhibition dominates sensory responses in the awake cortex. Nature *493*, 97–100.

Harris, K.D., and Shepherd, G.M. (2015). The neocortical circuit: themes and variations. Nat. Neurosci. *18*, 170–181.

Hallez, H., Vanrumste, B., Grech, R., Muscat, J., De Clercq, W., Vergult, A., D'Asseler, Y., Camilleri, K.P., Fabri, S.G., Van Huffel, S., et al. (2007). Review on solving the forward problem in EEG source analysis. J NeuroEngineering Rehabil. *4*, https://doi.org/10.1186/1743-0003-4-46.

Harris, J.A., Hirokawa, K.E., Sorensen, S.A., Gu, H., Mills, M., Ng, L.L., Bohn, P., Mortrud, M., Ouellette, B., Kidney, J., et al. (2014). Anatomical characterization of Cre driver mice for neural circuit mapping and manipulation. Front. Neural Circuits *8*, 76.

Hudetz, A.G. (2012). General anesthesia and human brain connectivity. Brain Connect. *2*, 291–302.

Imas, O.A., Ropella, K.M., Ward, B.D., Wood, J.D., and Hudetz, A.G. (2005). Volatile anesthetics disrupt frontal-posterior recurrent information transfer at gamma frequencies in rat. Neurosci. Lett. *387*, 145–150.

Katz, Y., Yizhar, O., Staiger, J., and Lampl, I. (2013). Optopatcher–an electrode holder for simultaneous intracellular patch-clamp recording and optical manipulation. J. Neurosci. Methods *214*, 113–117.

Kim, C.H., Lee, J., Lee, J.Y., and Roche, K.W. (2008). Metabotropic glutamate receptors: phosphorylation and receptor signaling. J. Neurosci. Res. *86*, 1–10.

Kim, E.J., Juavinett, A.L., Kyubwa, E.M., Jacobs, M.W., and Callaway, E.M. (2015). Three Types of Cortical Layer 5 Neurons That Differ in Brain-wide Connectivity and Function. Neuron *88*, 1253–1267.

Krashes, M.J., Koda, S., Ye, C., Rogan, S.C., Adams, A.C., Cusher, D.S., Maratos-Flier, E., Roth, B.L., and Lowell, B.B. (2011). Rapid, reversible activation of AgRP neurons drives feeding behavior in mice. J. Clin. Invest. *121*, 1424–1428.

Labarrera, C., Deitcher, Y., Dudai, A., Weiner, B., Kaduri Amichai, A., Zylbermann, N., and London, M. (2018). Adrenergic Modulation Regulates the Dendritic Excitability of Layer 5 Pyramidal Neurons In Vivo. Cell Rep. *23*, 1034–1044.

Larkum, M. (2013). A cellular mechanism for cortical associations: an organizing principle for the cerebral cortex. Trends Neurosci. *36*, 141–151.

Larkum, M.E., Zhu, J.J., and Sakmann, B. (2001). Dendritic mechanisms underlying the coupling of the dendritic with the axonal action potential initiation zone of adult rat layer 5 pyramidal neurons. J. Physiol. *533*, 447–466.

Larkum, M.E., Watanabe, S., Nakamura, T., Lasser-Ross, N., and Ross, W.N. (2003). Synaptically activated Ca2+ waves in layer 2/3 and layer 5 rat neocortical pyramidal neurons. J. Physiol. *549*, 471–488.

Lee, U., Ku, S., Noh, G., Baek, S., Choi, B., and Mashour, G.A. (2013). Disruption of frontal-parietal communication by ketamine, propofol, and sevoflurane. Anesthesiology *118*, 1264–1275.

Liu, X., Lauer, K.K., Ward, B.D., Rao, S.M., Li, S.J., and Hudetz, A.G. (2012). Propofol disrupts functional interactions between sensory and high-order processing of auditory verbal memory. Hum. Brain Mapp. *33*, 2487–2498.

Llinás, R., and Ribary, U. (2001). Consciousness and the brain. The thalamocortical dialogue in health and disease. Ann. N Y Acad. Sci. *929*, 166–175.

Madisen, L., Mao, T., Koch, H., Zhuo, J.M., Berenyi, A., Fujisawa, S., Hsu, Y.W., Garcia, A.J., 3rd, Gu, X., Zanella, S., et al. (2012). A toolbox of Cre-dependent optogenetic transgenic mice for light-induced activation and silencing. Nat. Neurosci. *15*, 793–802.

Mashour, G.A. (2014). Top-down mechanisms of anesthetic-induced unconsciousness. Front. Syst. Neurosci. *8*, 115.

Masri, R., Bezdudnaya, T., Trageser, J.C., and Keller, A. (2008). Encoding of stimulus frequency and sensor motion in the posterior medial thalamic nucleus. J. Neurophysiol. *100*, 681–689.

McCormick, D.A. (1993). Actions of acetylcholine in the cerebral cortex and thalamus and implications for function. Prog. Brain Res. *98*, 303–308.

McCormick, D.A., Pape, H.C., and Williamson, A. (1991). Actions of norepinephrine in the cerebral cortex and thalamus: implications for function of the central noradrenergic system. Prog. Brain Res. *88*, 293–305.

McGinley, M.J., Vinck, M., Reimer, J., Batista-Brito, R., Zagha, E., Cadwell, C.R., Tolias, A.S., Cardin, J.A., and McCormick, D.A. (2015). Waking State: Rapid Variations Modulate Neural and Behavioral Responses. Neuron *87*, 1143–1161.

Meyer, K. (2015). The role of dendritic signaling in the anesthetic suppression of consciousness. Anesthesiology *122*, 1415–1431.

Minnery, B.S., Bruno, R.M., and Simons, D.J. (2003). Response transformation and receptive-field synthesis in the lemniscal trigeminothalamic circuit. J. Neurophysiol. *90*, 1556–1570.

Muñoz, W., Tremblay, R., and Rudy, B. (2014). Channelrhodopsin-assisted patching: in vivo recording of genetically and morphologically identified neurons throughout the brain. Cell Rep. *9*, 2304–2316.

Muñoz, W., Tremblay, R., Levenstein, D., and Rudy, B. (2017). Layer-specific modulation of neocortical dendritic inhibition during active wakefulness. Science *355*, 954–959.

Murayama, M., Pérez-Garci, E., Nevian, T., Bock, T., Senn, W., and Larkum, M.E. (2009). Dendritic encoding of sensory stimuli controlled by deep cortical interneurons. Nature *457*, 1137–1141.

Nagel, G., Szellas, T., Huhn, W., Kateriya, S., Adeishvili, N., Berthold, P., Ollig, D., Hegemann, P., and Bamberg, E. (2003). Channelrhodopsin-2, a directly light-gated cation-selective membrane channel. Proc. Natl. Acad. Sci. USA *100*, 13940–13945.

Polack, P.O., Friedman, J., and Golshani, P. (2013). Cellular mechanisms of brain state-dependent gain modulation in visual cortex. Nat. Neurosci. *16*, 1331–1339.

Potez, S., and Larkum, M.E. (2008). Effect of common anesthetics on dendritic properties in layer 5 neocortical pyramidal neurons. J. Neurophysiol. *99*, 1394–1407.

Rockland, K.S. (1998). Complex microstructures of sensory cortical connections. Curr. Opin. Neurobiol. *8*, 545–551.

Ross, W.N. (2012). Understanding calcium waves and sparks in central neurons. Nat. Rev. Neurosci. *13*, 157–168.

Saalmann, Y.B., Pinsk, M.A., Wang, L., Li, X., and Kastner, S. (2012). The pulvinar regulates information transmission between cortical areas based on attention demands. Science *337*, 753–756.

Schaefer, A.T., Larkum, M.E., Sakmann, B., and Roth, A. (2003). Coincidence detection in pyramidal neurons is tuned by their dendritic branching pattern. J. Neurophysiol. *89*, 3143–3154.

Schmitt, L.I., Wimmer, R.D., Nakajima, M., Happ, M., Mofakham, S., and Halassa, M.M. (2017). Thalamic amplification of cortical connectivity sustains attentional control. Nature *545*, 219–223.

Schneider, C.A., Rasband, W.S., and Eliceiri, K.W. (2012). NIH Image to ImageJ: 25 years of image analysis. Nature Methods *9*, 671–675.

Sherman, S.M. (2014). The function of metabotropic glutamate receptors in thalamus and cortex. Neuroscientist *20*, 136–149.

Suzuki, M., and Larkum, M.E. (2017). Dendritic calcium spikes are clearly detectable at the cortical surface. Nat. Commun. *8*, 276.

Taniguchi, H., He, M., Wu, P., Kim, S., Paik, R., Sugino, K., Kvitsiani, D., Fu, Y., Lu, J., Lin, Y., et al. (2011). A resource of Cre driver lines for genetic targeting of GABAergic neurons in cerebral cortex. Neuron *71*, 995–1013.

Tononi, G., Boly, M., Massimini, M., and Koch, C. (2016). Integrated information theory: from consciousness to its physical substrate. Nat. Rev. Neurosci. *17*, 450–461.

Williams, S.R., and Fletcher, L.N. (2019). A Dendritic Substrate for the Cholinergic Control of Neocortical Output Neurons. Neuron *101*, 486–499.e4.

Williams, L.E., and Holtmaat, A. (2019). Higher-Order Thalamocortical Inputs Gate Synaptic Long-Term Potentiation via Disinhibition. Neuron *101*, 91–102.e4.

Williams, S.R., and Stuart, G.J. (1999). Mechanisms and consequences of action potential burst firing in rat neocortical pyramidal neurons. J. Physiol. *521*, 467–482.

Wilson, C.J., and Kawaguchi, Y. (1996). The origins of two-state spontaneous membrane potential fluctuations of neostriatal spiny neurons. J. Neurosci. *16*, 2397–2410.

Wimmer, V.C., Bruno, R.M., de Kock, C.P., Kuner, T., and Sakmann, B. (2010). Dimensions of a projection column and architecture of VPM and POm axons in rat vibrissal cortex. Cereb. Cortex *20*, 2265–2276.

Yu, W., Kwon, J., Sohn, J.W., Lee, S.H., Kim, S., and Ho, W.K. (2018). mGluR5-dependent modulation of dendritic excitability in CA1 pyramidal neurons mediated by enhancement of persistent Na^+ currents. J. Physiol. *596*, 4141–4156.

Zhou, H., Schafer, R.J., and Desimone, R. (2016). Pulvinar-Cortex Interactions in Vision and Attention. Neuron *89*, 209–220.

STAR★METHODS

KEY RESOURCES TABLE

REAGENT or RESOURCE	SOURCE	IDENTIFIER
Virus Strains		
pAAV-EF1a-double floxed-hChR2(H134R)-EYFP-WPRE-HGHpA	University of Pennsylvania Viral Vector Core or Addgene	Addgene AAV1; 20298-AAV1
pAAV-CaMKIIa-hChR2(H134R)-EYFP	University of Pennsylvania Viral Vector Core or Addgene	Addgene AAV1; 26969-AAV1
pAAV-hSyn-DIO-hM4D(Gi)-mCherry	Krashes et al., 2011	Addgene AAV9; 44362-AAV9
Chemicals		
D-APV	Tocris Bioscience	CAS: 79055-68-8
CNQX	Tocris Bioscience	CAS: 115066-14-3
CNO	Tocris Bioscience	CAS: 34233-69-7
TTX citrate	Tocris Bioscience	CAS: 18660-81-6
Atropine	Sigma-Aldrich	Cat#: 1045009
Mecamylamine	Sigma-Aldrich	Cat#: M9020
Nifedipine	Sigma-Aldrich	Cat#: N7634
Yohimbine	Sigma-Aldrich	Cat#: Y3125
Propranolol	Sigma-Aldrich	Cat#: P0884
Prazosin	Sigma-Aldrich	Cat#: P7791
TMP	Sigma-Aldrich	Cat#: T7883
Gabazine	Tocris Bioscience	CAS: 104104-50-9
MCPG	Sigma-Aldrich	Cat#: M4796
DiI	Invitrogen	Cat#: V22885
Fluorescent muscimol	Invitrogen	Cat#: M23400
Experimental Models: Organisms/Strains		
Mouse: Rbp4-KL100	Gong et al., 2007	RRID: MMRRC_031125-UCD
Mouse: Sim1-KJ18	Gerfen et al., 2013	RRID: MMRRC_031742-UCD
Mouse: Ai32	Madisen et al., 2012	RRID: JAX 012569
Mouse Rasgrf2-2A-dCre	Harris et al., 2014	RRID: JAX 022864
Mouse: SST-IRES-Cre	Taniguchi et al., 2011	RRID: JAX 013044
Software and Algorithms		
MATLAB	Mathworks	https://www.mathworks.com
ImageJ	Schneider et al., 2012	https://imagej.nih.gov/ij/

LEAD CONTACT AND MATERIALS AVAILABILITY

Further information and requests for resources should be directed to and will be fulfilled by the Lead Contact, Mototaka Suzuki (mototaka@gmail.com). This study did not generate new unique reagents.

EXPERIMENTAL MODEL AND SUBJECT DETAILS

Five transgenic mouse lines Rbp4-Cre (MMRRC 031125-UCD) (Gong et al., 2007), Sim1-Cre (MMRRC 031742) (Gerfen et al., 2013), Sim1-Cre × Ai32 (Rosa26-ChR2 reporter mice, JAX 012569) (Madisen et al., 2012), Rasgrf2-2A-dCre (JAX 022864) (Harris et al., 2014) and SST-IRES-Cre (JAX 013044) (Taniguchi et al., 2011) were used in this study. The age of studied mice was P40-70. Both male and female mice were used. No food or water restriction was imposed. All studied mice were in good health. Mice were housed in single-sex groups. Mice were housed in plastic cages with disposable bedding on a 12 hour light/dark cycle with food and water available *ad libitum*. Experiments were done during both dark and light phase. All procedures were approved and conducted in accordance with the guidelines given by the veterinary office of Landesamt für Gesundheit und Soziales Berlin.

METHOD DETAILS

Virus injection

Rbp4-Cre, Sim1-Cre, Rasgrf2-2A-dCre and SST-IRES-Cre mice were initially anesthetized with Isoflurane (1%–2.5% in O_2 vol/vol, Abbott) before ketamine/xylazine anesthesia (75/10 mg per kg of body weight, respectively) was administered intraperitoneally. Lidocaine (1% wt/vol, Braun) was injected around the surgical site. Body temperature was maintained at ~36°C by a heating pad and the depth of anesthesia was monitored throughout the virus injection. Once anesthetized, the head was stabilized in a stereotaxic instrument (SR-5R, Narishige, Tokyo). The skull was exposed by a skin incision and a small hole (~0.5 × 0.5 mm^2) was made above the hindlimb area of the primary somatosensory cortex (0.5 mm posterior to bregma and 1.5 mm from midline), the frontal cortex (1.0 mm anterior to bregma and 1.0 mm from midline) or the visual cortex (3.0 mm posterior to bregma and 2.5 mm from midline). AAV1.EF1a.DIO.hChR2(H134R)-eYFP.WPRE.hGH (Addgene 20298) from the University of Pennsylvania Viral Vector Core or Addgene was injected to Rbp4-Cre, Sim1-Cre and Rasgrf2-2A-dCre mice. AAV1.CaMKIIa. hChR2(H134R)-eYFP (Addgene 26969) from the University of Pennsylvania Viral Vector Core or Addgene and AAV9-hSyn-DIO-hM4D(Gi)-mCherry (Addgene 44362) from Addgene was injected to SST-IRES-Cre. Each construct was backloaded into a glass micropipette (Drummond) and was slowly injected (at 20 mL per min, total amount 40-50 nL to L5 for ChR2, total amount 100 nL to 300 m and 700 μm deep for DREADD). The pipette remained there for another 2-5 min after injection. The skin was sutured after retracting the pipette. Rasgrf2-2A-dCre mice were subsequently injected with trimethoprim (TMP, 150 μg per g of body weight) intraperitoneally.

Layer-specific optical stimulation

A custom-made μPeriscope (Suzuki and Larkum, 2017) whose tip was a 0.1 × 0.1 mm^2 or 0.18 × 0.18 mm^2 right-angle prism was inserted to L1 for stimulating the distal apical dendrites of L5 pyramidal neurons with blue light (λ = 473 nm). The timing of the optical stimulation was controlled by Power1401 and Spike2 software (CED) and synchronized with the neural recording system via TTL signals. The light intensity was varied between 2-12 mW/mm^2 whereas the duration was kept 20 ms.

Extracellular recordings

Animals were initially anesthetized by Isoflurane (1% in O_2, vol/vol, Abbott). For comparing anesthetic agents, either urethane (0.05 mg per kg of body weight, n = 3 mice) or ketamine/xylazine (75/10 mg per kg of body weight, respectively, n = 3 mice) was injected intraperitoneally. Lidocaine (1%, wt/vol, Braun) was injected around the surgical site. Body temperature was maintained at ~36 degrees by a heating pad and the depth of anesthesia was monitored throughout the experiment. Once anesthetized, the head was stabilized in the stereotaxic instrument and the skull was exposed by a skin incision. A ~1 × 1 mm^2 craniotomy was made above the hindlimb area of the primary somatosensory cortex (0.5 mm posterior to bregma and 1.5 mm from midline), the frontal cortex (1.0 mm anterior to bregma and 1.0 mm from midline), the visual cortex (3.0 mm anterior to bregma and 2.5 mm from midline), the posteromedial and pulvinar thalamic nucleus (1.8 mm posterior to bregma and 1.2 mm from midline) and/or the ventral posteromedial thalamic nucleus (1.8 mm posterior to bregma and 1.7 mm from midline). A pair of tungsten microelectrodes (one at 700 μm deep, the other at 200 μm deep) and a μPeriscope inserted to L1 were fixed to the skull with dental cement if mice were subsequently allowed to freely move in a rectangular arena (60 cm × 40 cm). For head-fixed animals, an aluminum head implant was fixed to the skull with dental cement; a single glass pipette or a 16 channel probe (ASSY-1, Cambridge NeuroTech, Cambridge) and a μPeriscope were independently inserted by micromanipulators (SM-15M, Narishige, Tokyo). For awake recordings, animal behavior was monitored after Isoflurane was stopped. Recordings started only after active and natural movements of limbs, tail and whiskers were frequently observed. Animal behavior was monitored throughout recordings. For treadmill walking (Figure S5), mice were habituated to head-fixation and walking on a custom-designed motorized treadmill. In each trial a mouse walked on the treadmill for 4 s and the blue light through the μPeriscope was given at 2 s after the treadmill onset. To measure the coupling during quiet rest, recordings were made only when no spontaneous movement of limbs, tail and whiskers was measured. Electrical activity was bandpass filtered at 1-9 kHz, digitized at 10 kHz, amplified by ERP-27 system and Cheetah software (Neuralynx). The slow component of somatic activity was obtained by low-pass filtering the activity with the cutoff frequency of 100 Hz. The fast component was high-pass filtered (100-3 kHz). To measure the spike rate (Figures 6 and S6), the highpass-filtered activity was thresholded by 3 × standard deviation. Evoked potentials were normalized by the pre-stimulus activity (−10 to 0 ms after light onset) and averaged over 50-70 measurements.

Optopatcher recordings

Animals were initially anesthetized by isoflurane (1% in O_2, vol/vol, Abbott). A μPeriscope inserted to L1 and an aluminum head implant were fixed to the skull with dental cement. Using an optopatcher (A-M Systems) (Katz et al., 2013; Muñoz et al., 2014), a patch clamp micropipette holder with an integrated optical fiber, a borosilicate glass pipette (2.0 mm outer diameter) containing normal rat ringer (135 mM NaCl, 5.4 mM KCl, 1.8 mM CaCl2, 1 mM MgCl2, 5 mM HEPES) was angled at ~45 degrees and inserted to the cortex with positive pressure (50-80 mbar) and advanced slowly (~5 μm per second) to the target depth of L5 (600-750 μm). Positive pressure was reduced to 30-40 mbar and the electrode advanced more slowly (1 μm per second) until a cell was encountered. Once the cell was isolated, its response to 20 ms light pulse (λ = 473 nm) from the in-pipette optical fiber was measured. If the cell showed robust, short-latency APs (see Figure S3), the positive pressure was released and slight suction was applied to establish a

stable loose seal (10-40 MΩ). If successful, its response to light stimulation (λ = 473 nm) through the μPeriscope pointing distal apical dendrites was measured. If the cell showed either no AP or delayed, transient APs in response to the light through the pipette, the cell was not studied further and the search for another cell resumed (Muñoz et al., 2014). Electrical activity was measured using Dagan BVC-700A amplifier and was filtered at 10 kHz.

Pharmacology

All drugs used in this study were prepared on the day of experiment, backloaded into a micropipette (Drummond) and slowly injected (at 20 nL per min, total 40-100 nl) to each target area. The pipette was angled 20-30 degrees to minimize damaging the dendrites under study. To block acetylcholine receptors (Figures 5A–5E), Atropine sulfate (muscarinic receptor antagonist, 1045009) and Mecamylamine (nicotinic receptor antagonist, M9020) were used (both 1 mM from Sigma Aldrich). To block noradrenergic receptors (Figures 5A–5E), Prazosin (α1-receptor antagonist, P7791), Yohimbine (α2-receptor antagonist, Y3125) and Propranolol (β1- & β2-receptor antagonist, P0884) were mixed (all 1 mM from Sigma Aldrich). Fluorescent muscimol (M23400) and DiI (V22885) was purchased from Invitrogen. TMP (T7883), MCPG (M4796) and Nifedipine (N7634) were from Sigma Aldrich. APV (0106), TTX citrate (1069), CNQX (CAS: 115066-14-3), Gabazine (CAS: 104104-50-9) and CNO (CAS: 34233-69-7) were from Tocris. Parameters such as concentration, volume, speed of injection were based on the previous studies (Constantinople and Bruno, 2011; Guo et al., 2017; Larkum et al., 2003; Murayama et al., 2009; Polack et al., 2013) and our own tests.

Sensory stimulation

The mice were anesthetized with 1% Isoflurane. Sensory stimulation (Figures S1A and S6F) was provided by a single air puff given to the contralateral hindpaw or whiskers. The air puff was generated by briefly (20-50 ms) opening a valve (Takasago Electric, RP-Q1) via TTL signals.

QUANTIFICATION AND STATISTICAL ANALYSIS

MATLAB (Mathworks) was used for data analysis. The sample sizes are similar to those used in the field. No statistical methods were used to determine sample size. We did not exclude any animal for data analysis. Trials with different light intensities were randomly interleaved. All comparisons using Student's t tests or nonparametric Wilcoxon tests were two-sided and each test was selected based on the data distribution histogram.

DATA AND CODE AVAILABILITY

Data are available upon request from the Lead Contact, Mototaka Suzuki (mototaka@gmail.com).

Supplemental Figures

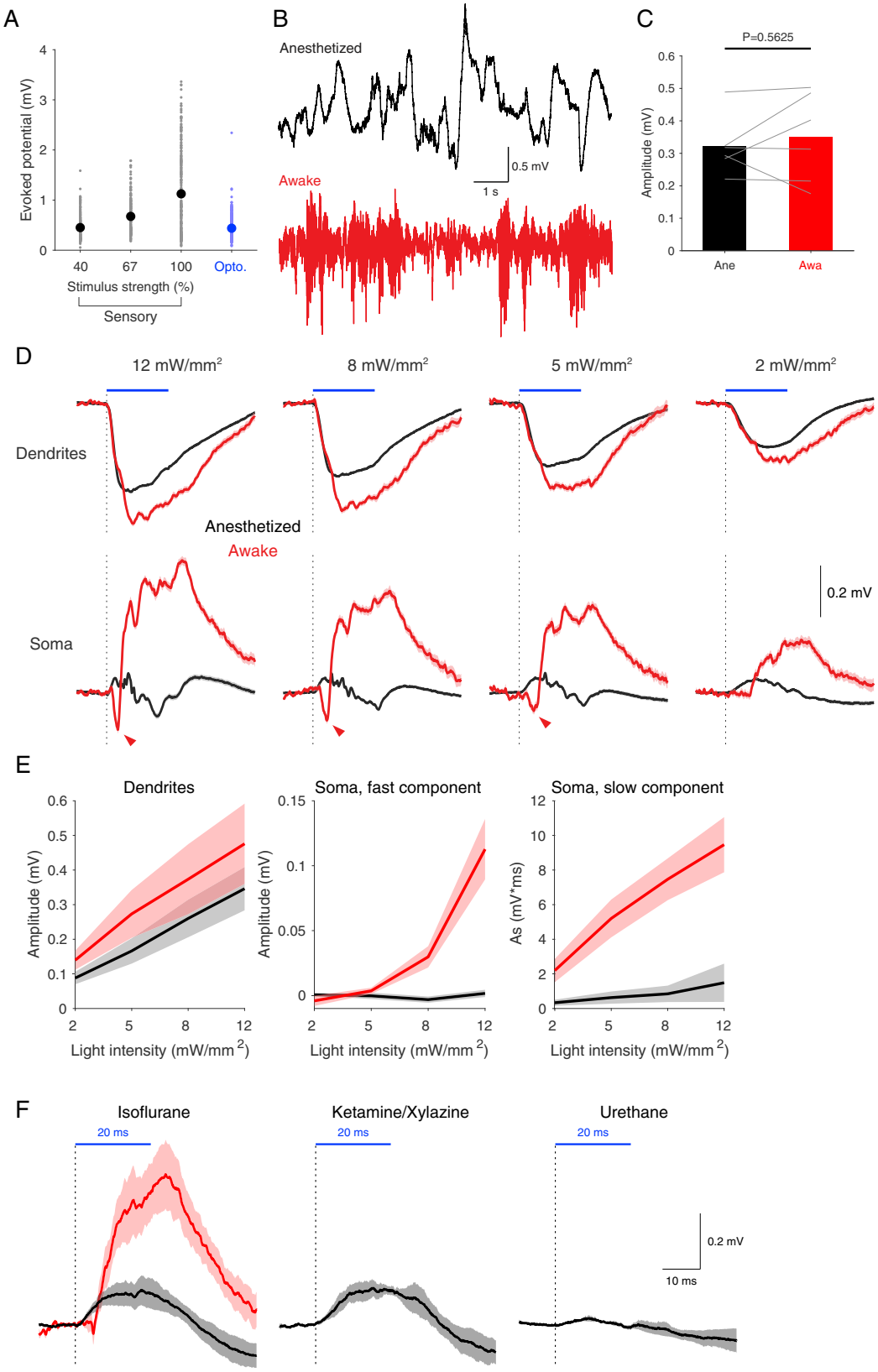

(legend on next page)

Figure S1. Dendritic and Somatic Responses during Anesthesia and Wakefulness, Related to Figure 1

(A) Dendritic responses to optogenetic stimulation are in the physiological range with similar amplitudes compared to sensory evoked potentials. The peak amplitudes of evoked potential were measured at the same cortical depth (200 μm deep from pia) in the same area (the hindlimb area in the primary somatosensory cortex) in response to air puff (black, n = 3 mice) or optogenetic stimulation with the μPeriscope (blue, n = 6 mice, at maximum intensity of 12 mW/mm^2).

(B) Spontaneous field potentials in L5 during anesthetized (black) and awake (red) states. Data were obtained from the same mouse and electrode.

(C) Dendritic response did not significantly change depending on the conscious state. Evoked potentials were measured at 200 μm deep from pia (n = 6 mice, 40-70 measurements from each mouse). Peak amplitudes did not significantly differ depending on the conscious state (p = 0.5625, Wilcoxon signed rank test, n = 6 mice).

(D) Decoupling during anesthesia over different light intensities. Average field potential at distal apical dendrites (200 μm deep from pia) and soma (700 μm deep) from one mouse. Arrow heads indicate the fast somatic spikes. Blue line indicates the duration of blue light (20 ms). Shading indicates SEM.

(E) Summary of (D) (n = 4 mice, mean ± SEM).

(F) Dendro-somatic decoupling during anesthesia is independent of anesthetic agent. Average field potentials recorded in L5 (700 μm deep from pia) during wakefulness (left in red, n = 5 mice) and when anesthetised with 1% Isoflurane (left in black, n = 5 mice), Ketamine/Xylazine (middle, n = 3 mice) or Urethane (right, n = 3 mice). Shading indicates SEM.

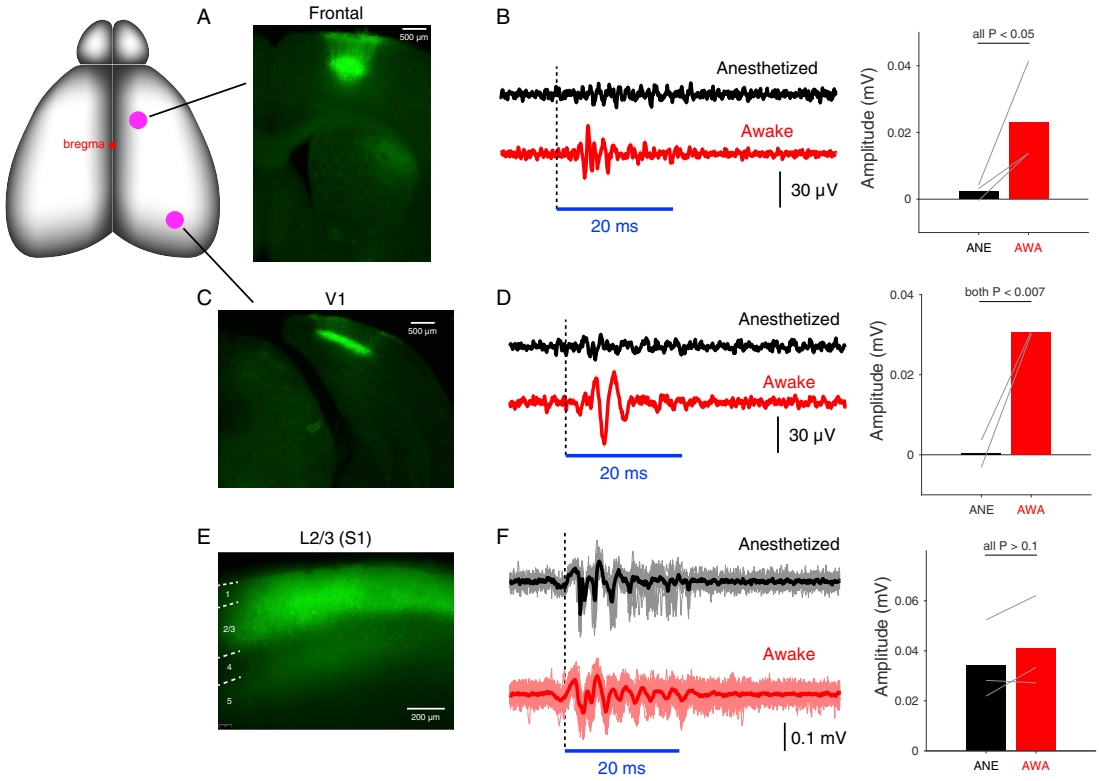

Figure S2. Anesthetic-Induced Decoupling of L5 Pyramidal Neurons in Other Cortical Areas, Related to Figure 1

(A) A fluorescence image of the slice containing the frontal cortex where L5 pyramidal neurons express ChR2 and YFP.

(B) In all n = 3 mice, the fast somatic activity was significantly elevated during wakefulness compared to anesthetized states (all $p < 0.05$, Wilcoxon rank sum test).

(C) A fluorescence image of the slice containing V1 where L5 pyramidal neurons express ChR2 and YFP.

(D) In both mice (n = 2), the fast somatic activity was significantly elevated during wakefulness compared to anesthetized states (both $p < 0.007$, Wilcoxon rank sum test). In each condition evoked potentials were averaged over 50-70 measurements.

(E) A fluorescence image of the cortical slice where L2/3 neurons express ChR2 (green).

(F) In all n = 3 mice, the fast somatic responses during anesthetized and awake states were not significantly different (all $p > 0.1$, Wilcoxon rank sum test). In each condition evoked potentials were averaged over 50-70 measurements.

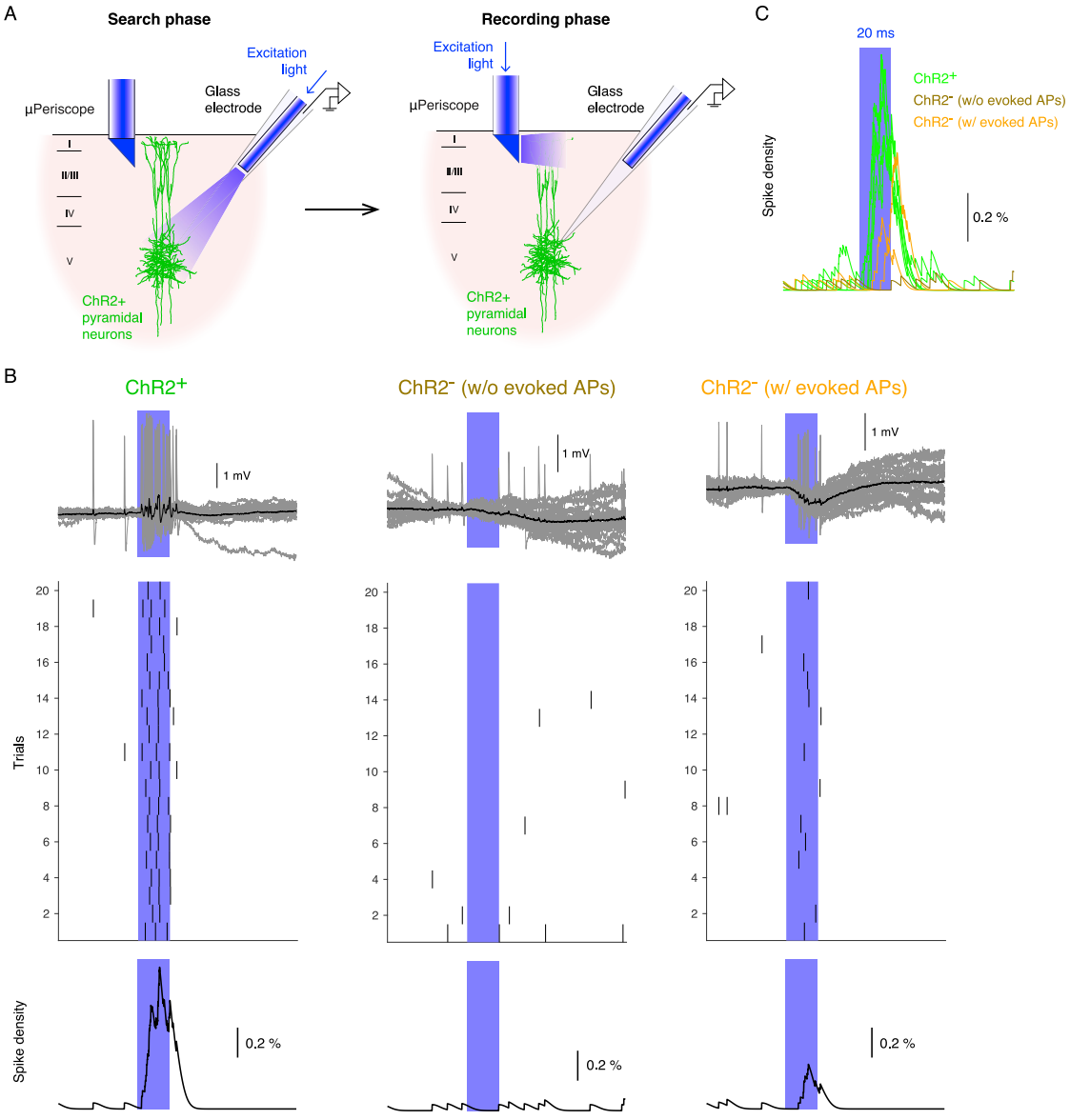

Figure S3. Juxtacellular Recording with an Optopatcher, Related to Figure 2

(A) Schematic diagram of the experiment. While searching for a ChR2$^+$ neuron, neuronal responses to the direct light through the in-pipette optical fiber were examined (left). If the isolated cell was judged to be ChR2$^+$, somatic responses to dendritic stimulation through μPeriscope were measured (right).

(B) Top: Action potentials evoked by the direct light through the in-pipette optical fiber in a ChR2$^+$ cell (left), ChR2$^-$ cell without evoked APs (middle) and ChR2$^-$ cell with occasionally evoked APs (right). Individual traces in gray; average in black. Middle: Raster plots of action potentials over trials. Bottom: Corresponding spike density functions (convoluted with a half-Gaussian function with σ = 5 ms). Blue shading indicates the duration of light stimulation (20 ms).

(C) Summary of (B) (five ChR2$^+$ cells, one ChR2$^-$ cell without evoked APs and two ChR2$^-$ cells with occasionally evoked APs from four mice).

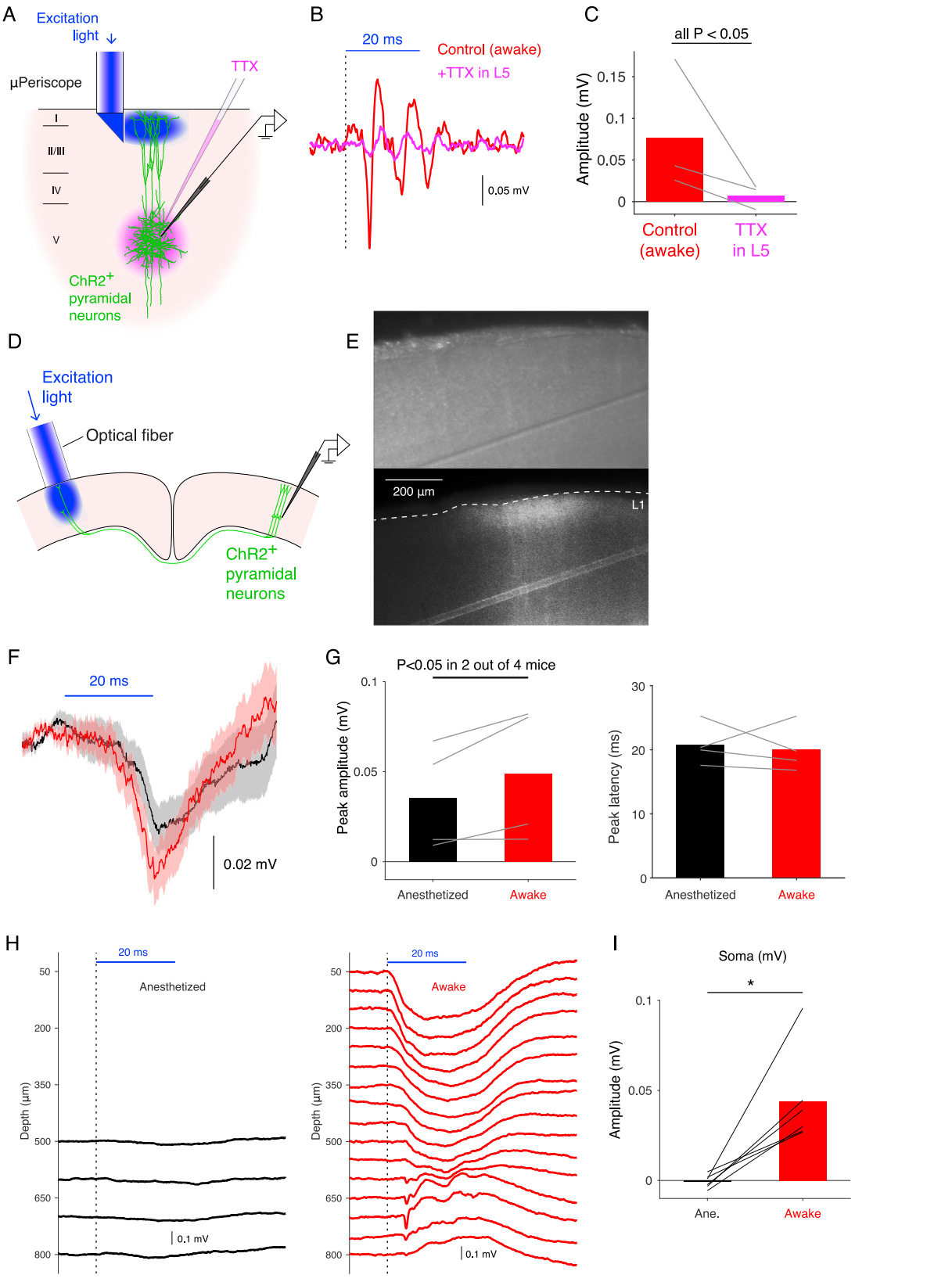

(legend on next page)

Figure S4. The Fast Somatic Component Represents APs, Related to Figure 2

(A) Schematic diagram of the TTX experiment.

(B) Average fast somatic component of field potential in L5 before and after 3 μM TTX application (50 nL) in L5.

(C) Summary of (B) ($p < 0.05$ in all $n = 3$ mice, two-sided Wilcoxon rank sum test).

(D) Schematic diagram of the experiment where antidromically evoked potentials were measured in both anesthetized and awake states.

(E) A cortical slice of the contralateral (optically stimulated) hemisphere. Upper: bright field, lower: fluorescence image of ChR2-eYFP.

(F) Antidromically evoked potentials in awake (red) and anesthetized states (black) from one animal. Shading indicates SEM.

(G) The peak amplitude of antidromically evoked potentials significantly increased during wakefulness in 2 out of 4 mice ($p < 0.05$, two-sided Wilcoxon rank sum test) and the peak latency was very similar in 4 mice.

(H) Example laminar profile in anesthetized (left) and awake states (right) from a Sim1-Cre mouse. Notice that prominent fast somatic spikes were observed during wakefulness (right at 700 μm deep) but not at all during anesthesia (left). Each trace is the average over 50-70 measurements.

(I) Amplitudes of fast somatic spike in anesthetized and awake states ($n = 6$ mice, *$p = 0.0312$, Wilcoxon signed rank test).

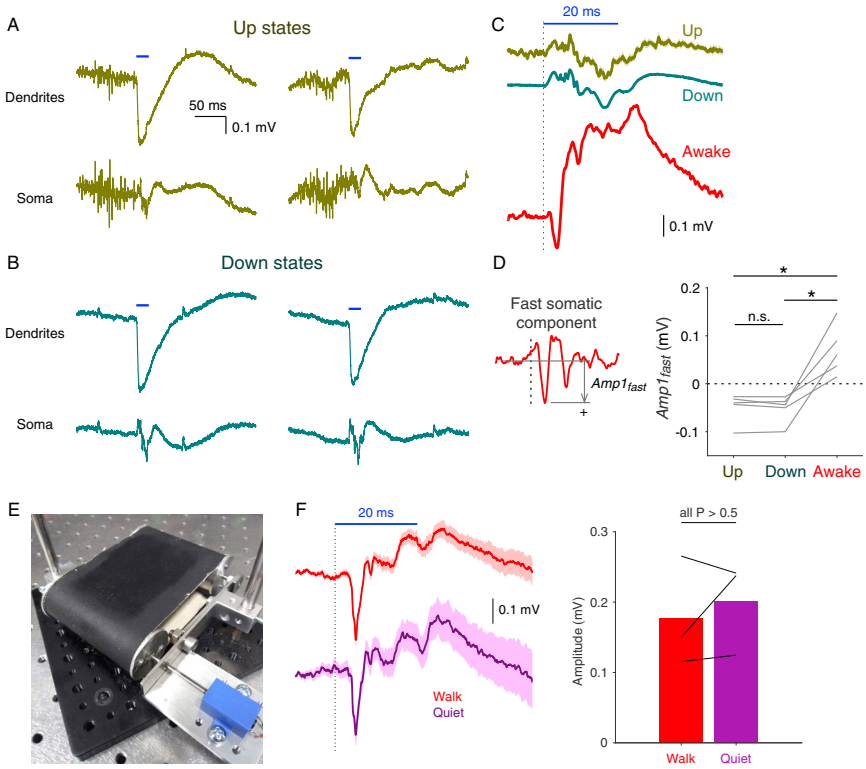

Figure S5. Coupling in Up and Down States during Anesthesia and during Active versus Quiet Wakefulness, Related to Figure 4

(A) Two example traces of dendritic and somatic responses in Up states. Blue bar indicates when the light was given to distal apical dendrites (20 ms).

(B) Same as (A) but in Down states.

(C) Average over all somatic responses in Up (top), Down (middle) and awake (bottom) states from the same animal. Shading indicates SEM.

(D) Fast somatic spike during awake states compared to the somatic responses averaged over the corresponding period (3-6 ms after the light onset) in Up and Down states during anesthesia. *$p < 0.05$, Kruskal-Wallis test with post hoc multiple comparison, $n = 5$ mice.

(E) The motorized treadmill used to examine the coupling during walking and quiet wakefulness.

(F) In all $n = 3$ mice, the fast somatic responses in the two awake states were not significantly different (all $p > 0.5$, Wilcoxon rank sum test). In each condition evoked potentials were averaged over 50-70 measurements.

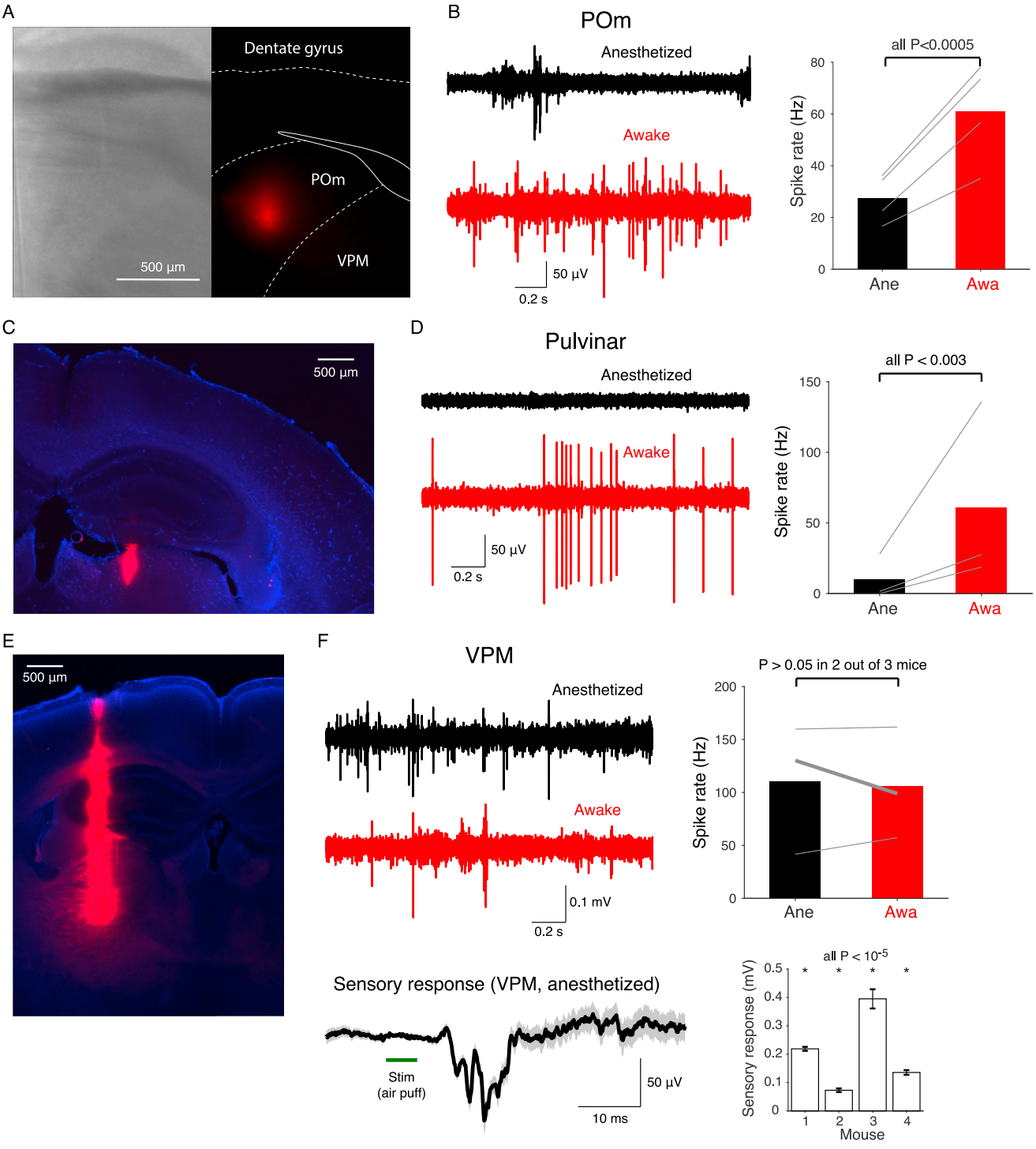

Figure S6. Thalamic Activity during Anesthesia and Wakefulness, Related to Figure 6

(A) Bright field image of POm (left) and DiI fluorescence image of the same slice showing the location of the 16-channel silicone probe tip (right). Scale bar indicates 500 µm.

(B) Example POm activity during anesthesia (top left) and wakefulness (bottom left) from the same mouse. Each trace was high-pass filtered with the cutoff frequency of 300 Hz. In all n = 4 mice, spontaneous spike rate in POm is significantly higher during wakefulness compared to anesthesia ($p < 0.0005$, Wilcoxon signed-rank test).

(C) DiI staining (red) confirmed the localization of recording electrode to Pulvinar.

(legend continued on next page)

(D) In all n = 3 mice, spontaneous Pulvinar activity was significantly elevated during wakefulness compared to anesthetized states (all $p < 0.003$, Wilcoxon rank sum test). (E) DiI staining (red) confirmed the localization of recording electrode to VPM.

(F) In 2 out of 3 mice, spontaneous VPM activity was not statistically different in anesthetized and awake states (top right, both $p > 0.05$, Wilcoxon rank sum test); in one mouse (thick gray line) VPM neurons were significantly less active in awake states ($p = 0.0195$, Wilcoxon rank sum test). VPM neurons strongly respond to sensory stimuli (air puff) during anesthesia (bottom, n = 4 mice, all $p < 10^{-5}$,Wilcoxon signed rank test).

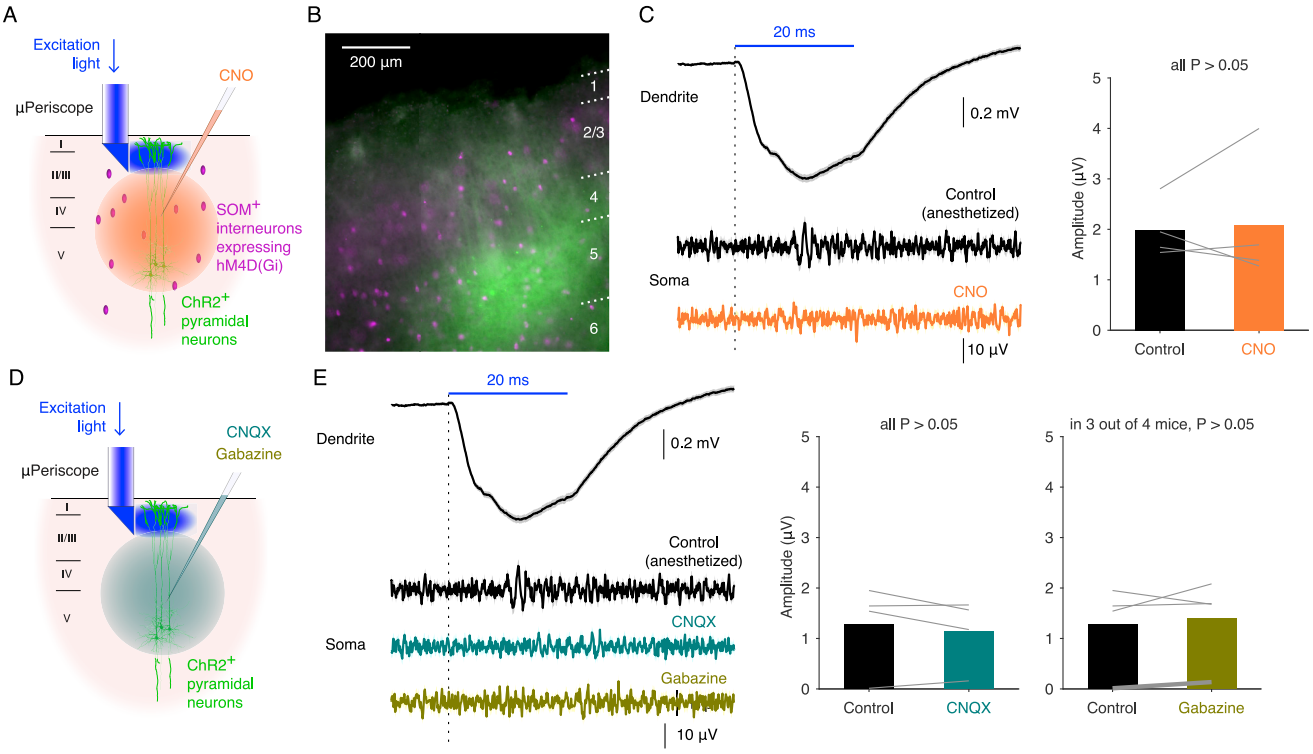

Figure S7. Examining the Contribution of Interneurons to Decoupling, Related to Figure 6

(A) Schematic diagram of the experiment inactivating SOM$^+$ interneurons.

(B) A fluorescence image of the cortical slice where L5 pyramidal neurons express ChR2-YFP (green) and SOM$^+$ interneurons express hM4D(Gi)-mCherry (magenta).

(C) Application of CNO (14 µM, 100 nL) did not enhance coupling of L5 pyramidal neurons (all $p > 0.05$, $n = 4$ mice, Wilcoxon rank sum test). In each condition evoked potentials were averaged over 50-70 measurements.

(D) Schematic diagram of the experiment blocking AMPA receptors or $GABA_A$ receptors.

(E) Application of AMPA receptor blocker CNQX (100 µM, 100 nL) or $GABA_A$ receptor blocker Gabazine (5 µM, 100 nL) did not enhance the coupling of L5 pyramidal neurons (CNQX: all $p > 0.05$, $n = 4$ mice, Wilcoxon

rank sum test; Gabazine: in 3 out of 4 mice $p > 0.05$, Wilcoxon rank sum test; in one mouse (thick gray line) $p = 0.048$, Wilcoxon rank sum test). In each condition evoked potentials were averaged over 50-70 measurements.